NEDO-21052-A
75NED53
CLASS I
MAY 1979

MAXIMUM DISCHARGE RATE OF LIQUID-VAPOR MIXTURES FROM VESSELS

F. J. MOODY

597 161

GENERAL ELECTRIC

NEDO-21052-A
75NED53
Class I
May 1979

MAXIMUM DISCHARGE RATE OF LIQUID-VAPOR MIXTURES FROM VESSELS

F. J. Moody

F. J. Moody
Nuclear Technology Department

Approved: H. E. Townsend

H. E. Townsend, Manager
Containment Methods

NUCLEAR ENERGY ENGINEERING DIVISION • GENERAL ELECTRIC COMPANY
SAN JOSE, CALIFORNIA 95125

597 162

GENERAL ELECTRIC

DISCLAIMER OF RESPONSIBILITY

597 163

PREFACE

This approved version of report NEDO-21052 (September 1975) is being provided in accordance with the NRC's topical report program. This report NEDO-21052-A consists of the original text of NEDO-21052, the NRC staff letter accepting this report as a reference, the NRC staff Topical Report Evaluation and the supplementary information General Electric provided to the NRC staff during the review of NEDO-21052.

TABLE OF CONTENTS

597 165

RECEIVED
JAN 0 5 1979
L.J. SOBON

UNITED STATES
NUCLEAR REGULATORY COMMISSION
WASHINGTON, D. C. 20555

DEC 27 1978

MFN-004-79

General Electric Company
ATTN: Mr. L. J. Sobon, Manager
BWR Containment Licensing MC905
175 Curtner Avenue
San Jose, CA 95125

Gentlemen:

SUBJECT: REVIEW OF GENERAL ELECTRIC TOPICAL REPORT NEDO-21052, "MAXIMUM DISCHARGE RATE OF LIQUID-VAPOR MIXTURES FROM VESSELS"

We have completed our review of the General Electric Topical Report NEDO-21052, "Maximum Discharge Rate of Liquid-Vapor Mixtures from Vessels," as it is to be applied to determine the mass and energy release rate resulting from a design basis accident for Mark I containment response analyses. Based on our review, we conclude that the model described in NEDO-21052, in conjunction with its method of application for Mark I containment response analyses, are acceptable for reference as specified in the enclosure.

During the course of our review, we determined that additional justification would be necessary to support application of this model to break sizes and types other than the double-ended rupture of a recirculation line in a Mark I plant. We understand that you wish to pursue the application of this model for other sizes and types of breaks. Therefore, when you provide the additional information required, as discussed in our letter dated January 30, 1978, the staff will continue its review of the subject topical report. Such information should be submitted to the Division of Project Management.

The staff does not intend to repeat its review of this topical report when it appears as a reference for a Mark I containment response analysis, except to assure that the model is applicable to the specific plants involved. Should the regulatory criteria or regulations change such that our conclusions concerning this topical report become invalid, you will be notified and will be given the opportunity to revise and resubmit your topical report for review, should you so desire.

597 166

- 2 -

In accordance with established procedure, we request that General Electric issue a revised version of the topical report to include any supplementary information provided for our review, this acceptance letter, and the NRC staff evaluation.

Sincerely,

Darrell Eisenhut

D. Eisenhut Acting Assistant
Director for Systems and
Projects,
Division of Operating Reactors

Enclosure:
Topical Report Evaluation

cc: Mr. L. Gifford
General Electric Company
4720 Montgomery Lane
Bethesda, MD 20014

597 167

MAXIMUM DISCHARGE RATE OF LIQUID-VAPOR MIXTURES FROM VESSELS

F.J. Moody

ABSTRACT

A discrepancy exists in theoretical predictions of the two-phase equilibrium discharge rate from pipes attached to vessels. Theory which predicts critical flow data in terms of pipe exit pressure and quality severely overpredicts flow rates in terms of vessel fluid properties. This study shows that the discrepancy is explained by the flow pattern. Due to decompression and flashing as fluid accelerates into the pipe entrance, the maximum discharge rate from a vessel is limited by choking of a homogeneous bubbly mixture. The mixture tends toward a slip flow pattern as it travels through the pipe, finally reaching a different choked condition at the pipe exit.

NOMENCLATURE

A	Area
fL/D	Pipe Friction Parameter
G	Mass Flux
g_c	Newton's Constant
h	Enthalpy
K	Slip Ratio
$\dot{m}_{ij}$, $\dot{m}_{ji}$	Vaporization or Condensation Rates
p	Pressure
s	Entropy
T	Temperature
u	Speed
V	Speed of Disturbance Propagation
v	Specific Volume
v^*	Specific Volume, Defined by Equation (18)
v_m	Specific Volume, Defined by Equation (24)
v_e	Specific Volume, Defined by Equation (25)
x	Flowing Quality
Z	Function Defined by Equation (42)
α	Void Fraction
θ	Entropy Production Function, Defined by Equation (39)

Subscripts

c	Critical Flow Rate
f	Saturated Liquid
g	Saturated Vapor
fg	Vaporization
o	Stagnation
REF	Reference Value

Superscript

'	Derivative with Respect to Pressure

Other Notation

in.	inch(es)
cm	centimeter(s)
m	meter(s)
sq	square
lbf	Pound(s) Force
lbm	Pound(s) Mass
kN	Kilonewton(s)
kgm	Kilogram(s)
Btu	British thermal unit(s)

INTRODUCTION

When high pressure fluid near the saturation state is discharged to a low pressure receiver, the mass flow rate will be limited to a maximum value which depends on conditions in the vessel. The discharge rate largely determines vessel decompression rate, receiver pressurization rate, vessel thrust reaction, and impingement forces on nearby objects. Prediction of the critical flow rate plays a major role in determining core cooling requirements associated with safety analyses of nuclear power plants.

Experimental programs conducted by numerous workers have provided a broad range of two-phase critical flow data (e.g., References 1 through 7). Geometries tested include orifices, nozzles, tubes, and pipes of various lengths and sizes. Liquid-vapor critical flow data fall into either *equilibrium* or *non-equilibrium* classifications; subdivisions include geometry and the flow pattern. The non-equilibrium classification has been studied in part by various workers including Henry (8, 9) and Edwards (10). However, Boure' (11) suggested that further progress in two-phase flow depends on additional study of phenomena which govern interfacial forces and transfer rates of heat and mass. Idealized equilibrium flows are less complex because they do not require theoretical models for interfacial heat and mass transfer.

A discrepancy associated with equilibrium flows is addressed in this study. It has been shown by Fauske (4) and Henry (6) that critical flow data is seriously underpredicted by the homogeneous model in terms of pipe exit static pressure and quality. On the other hand, slip flow models, including those by Fauske (4), Levy (12), and Moody (13) reasonably pre-

597 168

dict much of the pipe exit data, in spite of the fact that they satisfy either momentum or energy conservation, but not both, and hence do not completely describe two-phase critical flow. In seeming contradiction, others, including Allemann (14) and Moody (15), showed that slip flow models greatly overpredict two-phase blowdown rates in terms of vessel stagnation properties. This represents a fundamental discrepancy in theoretical prediction of two-phase critical flow. Whether slip models are inadequate for relating critical flow and stagnation properties, or whether the discrepancy is caused by other model difficulties needs to be understood. It is the purpose of this study to explain the discrepancy and provide a basis for accurately predicting the maximum discharge rate of equilibrium liquid-vapor mixtures from vessels.

EQUILIBRIUM TWO-PHASE FLOWS

Since this study is for equilibrium flows, it is necessary to identify physical constraints which determine saturated equilibrium for a two-phase critical flow. When liquid at equilibrium is decompressed below its saturation pressure, vapor is formed at a finite rate until a new equilibrium state is reached. Several studies have been made which help determine the duration of non-equilibrium states. Edwards and O'Brien (16) conducted experiments in which a 3.96 m (13 ft) long, 7.32 cm (2.88 in.) i.d. pipe was ruptured at one end after pressurization to 70 atmospheres. High-speed pressure recordings along the pipe showed that pressure dropped below the saturation value and rose again within 0.5 millisecond. Zaker and Wiedermann (17) employed a 5.08 cm (2 in.) i.d., 1.83 m (6 ft) long tube and found that non-equilibrium states lasted for less than 1 millisecond. The same duration of non-equilibrium states was found by Gallagher (18) during decompression experiments on 5.08 cm (2 in.) i.d. hot water driver tubes of 1.83, 3.66, and 5.18 m (6, 12, and 17 ft) length, pressurized up to 140 atmospheres and temperatures up to saturation. These water depressurization studies indicate that non-equilibrium states survive for a millisecond or less.

A fluid particle which is accelerated from stagnation in a vessel into a pipe will undergo rapid decompression. Based on the decompression studies mentioned, it is reasonable to expect that when moving in a decreasing pressure field, a fluid particle lags behind equilibrium about 1 millisecond in time. Once inside a uniform pipe, fluid acceleration and associated pressure reduction decrease, permitting equilibrium states to be closely approached if the pipe is sufficiently long. For example, the maximum water speed achievable from a system at 70 atmospheres is about 120 mps (400 fps). Therefore, the farthest a water particle can travel in 1 millisecond is about 12 cm (0.4 ft). It follows that if the flow path is less than 12 cm, non-equilibrium states are expected whereas in longer flow passages, equilibrium states are expected.

Fauske (19), Uchida (20), Simon (21), and Sutherland (7) have presented water bl[illegible] data for pipes of various lengths with dia[illegible] to 1.27 cm (0.5 in.). When the data for fix[illegible] conditions are plotted as a function of pipe length, a characteristic knee is observed near a length of 10 cm (4 in.). Pipes approaching zero length tend to have non-flashing orifice discharge rates. As pipe length is increased, the discharge rate decreases sharply. For pipe lengths greater than about 10 cm, the discharge rate is unaffected by further increase in pipe length. This observation is consistent with the time required for a steam-water system to approach saturated equilibrium. Data of Sozzi and Sutherland (7) for 1.27 cm (0.5 in.) i.d. pipes shows that even subcooled water in the vessel requires no more than 12.7 cm (5 in.) to approach equilibrium.

This study applies only to flow passages long enough to assure that equilibrium is approached. For hot water, that length is less than 12.7 cm (5 in.).

THE FLOW PATTERN

Since equations which govern two-phase flow differ in modeling relative motion between vapor and liquid, theoretical values of the critical flow rate strongly depend on the flow pattern. Various correlations have been proposed for predicting flow pattern in steady two-phase flow, some of which are summarized by Lahey (22) and Wallis (23). However, flow pattern correlations are not available for steep pressure gradients or unsteady decompression. When a body of liquid is decompressed below its saturation pressure, homogeneous boiling occurs. For example, photographs by Kober (24) show the formation of thoroughly mixed bubbles in liquid during the depressurization of hot water in glass vessels, initially pressurized to about 2 atmospheres. Furthermore, at high pressure, both Edwards (16) and Gallagher (18) found that transient water depressurization in long pipes was predicted by models based on homogeneous bubbles in liquid. Therefore, it is expected that when a particle of liquid is accelerated into the entrance of a discharge pipe, decompression below its saturation pressure will cause homogeneous boiling. If the flow path into a discharge pipe is short so that vapor formation is not complete, continued homogeneous boiling is expected until equilibrium is approached. Even though discrete bubbles move relative to liquid during acceleration, the homogeneous model is expected to describe pipe entrance conditions during blowdown. Moreover, homogeneous choked flow near the entrance may better represent blowdown data in terms of stagnation properties.

Inside the pipe, vapor formation rate is reduced, and transition to other flow patterns can occur. For steam-water critical flow in straight pipes, Fauske (4) determined from steady-state correlations that the annular flow pattern was most likely. Flow pattern studies by Henry (25) near the discharge of a straight pipe showed that the slip ratios were less than required for annular flow, but definitely indicated a slip flow. Even though the blowdown flow may be limited by homogeneous choking at the pipe entrance, transition to a slip flow could produce a second choked condition near the pipe exit. These two possible choked conditions are considered next.

CHOKED FLOW

Critical flow occurs when further reduction in receiver pressure does not change the mass discharge rate from a flow passage which is attached to a vessel. Mathematically, this condition corresponds to

$$\frac{dG}{dp} = 0 \tag{1}$$

The sonic state of a fluid occurs when further reduction in receiver pressure does not propagate into the flow. If V is the propagation speed of a dis-

169

turbance against the direction of flow, conditions for the sonic state are

$$V = \frac{dV}{dp} = 0 \tag{2}$$

When equations (1) and (2) are satisfied simultaneously, the flow is choked. Equation (2) also characterizes steady flow conditions when no disturbances are present.

THE HOMOGENEOUS MODEL

Although homogeneous theory is well established, several important features of choked flow are summarized here. The one-dimensional conservation equations written for a small disturbance moving at absolute speed, V, against a homogeneous, frictionless, adiabatic flow are,

$$\text{Mass:} \quad d(GA) + d(AV/v) = 0 \tag{3}$$

$$\text{Momentum:} \quad d(G^2Av) + d(AV/v) + g_c A dp = 0 \tag{4}$$

$$\text{Energy:} \quad d(GAh_o) + d(AVh_o/v) - AVdp = 0 \tag{5}$$

Employing the definition of stagnation enthalpy,

$$h_o = h + G^2v^2/2g_c \tag{6}$$

equations (3), (4), and (5) are combined with the Gibbs equation to show that

$$Tds = dh - vdp = 0. \tag{7}$$

It follows that state changes occur isentropically across the disturbance. For steady flow it is similarly shown that state changes are isentropic.

If the sonic conditions of equation (2) exist somewhere in the flow, and steady flow occurs upstream, equations (3) and either (4) or (5) are integrated at constant entropy from stagnation to a condition where equation (1) is satisfied, for which

$$G = \sqrt{-g_c\left(\frac{\partial p}{\partial v}\right)_s} \tag{8}$$

Equation (8) is the well known expression for critical flow of a homogeneous fluid, which can be shown to occur simultaneously with the sonic state either in the throat of a converging-diverging nozzle or in a uniform area flow passage.

Computations giving the critical mass flux and critical flow pressure for a homogeneous steam-water mixture are graphed in Figures 1 and 2 in terms of stagnation pressure and enthalpy. Both subcooled and saturated states are shown.

A CONSISTENT SLIP MODEL

Whether or not critical flow and sonic states occur simultaneously for flow patterns other than homogeneous has been questioned. Faletti (1) noted that at maximum steam-water flows, further reduction of receiver pressure slightly affected pressures inside the flow passage. Isbin (3) suggested that in annular flow, pressure disturbances might propagate upstream in the liquid film. However, Henry (25) concluded that two-dimensional effects near the exit of two-phase critical discharge explained apparent receiver pressure influence for short distances upstream. He found that these effects could be reduced with gradual rather than abrupt expansion at the pipe exit. It is shown in this section that for

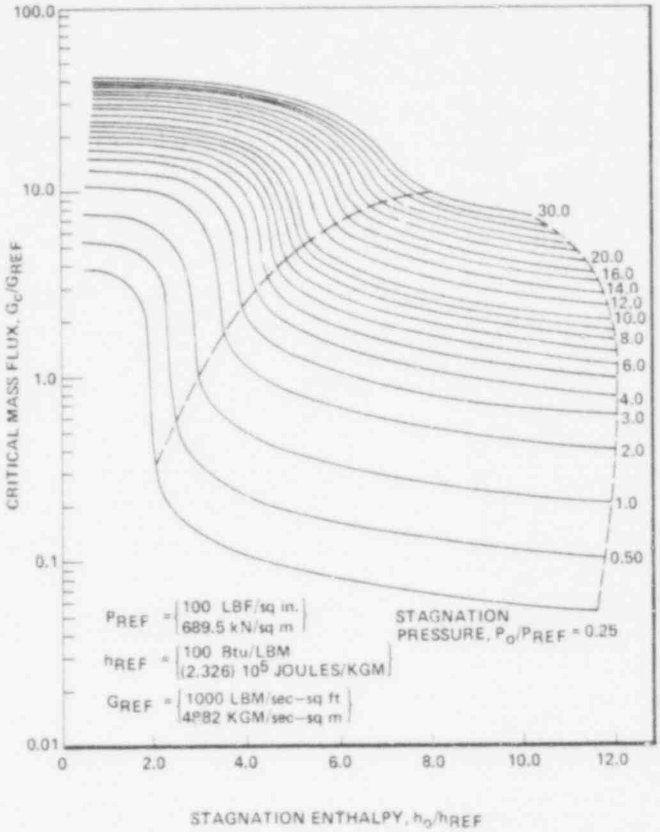

Fig.1 Critical mass flux - homogeneous, equilibrium steam-water

an idealized one-dimensional slip model, critical flow and sonic states can occur simultaneously.

Several two-phase slip models for critical flow by Fauske (4), Levy (12), and Moody (13) are based on either momentum or energy conservation, but not both, and hence are not consistent. Since the slip ratio introduced one more degree of freedom, additional assumptions were imposed, such as isentropic or isenthalpic flow. These assumptions do not necessarily describe the physical behavior.

This study includes all the conservation laws, and hence is consistent. The slip model developed here is described by separated streams of liquid and vapor in saturated equilibrium undergoing one-dimensional flow at average, unequal speeds. Momentum and kinetic energy transport due to phase change at the interface is based on speed of the initial phase, whereas transport of enthalpy and entropy is based on the final phase. These idealizations primarily affect vaporization and condensation rates. Heat transfer and shear stress at the wall, and interfacial shear stress are considered negligible.

Following a procedure similar to that for homogeneous flow, mass, momentum, and energy conservation equations for each phase are written for a small disturbance moving leftward at absolute speed V in a passage of variable area, into steady slip flow to the right. Subscripts i and j refer to either the liquid or vapor. When i and j both appear in an expression, i ≠ j. Derivations are given in Appendix I.

597 170

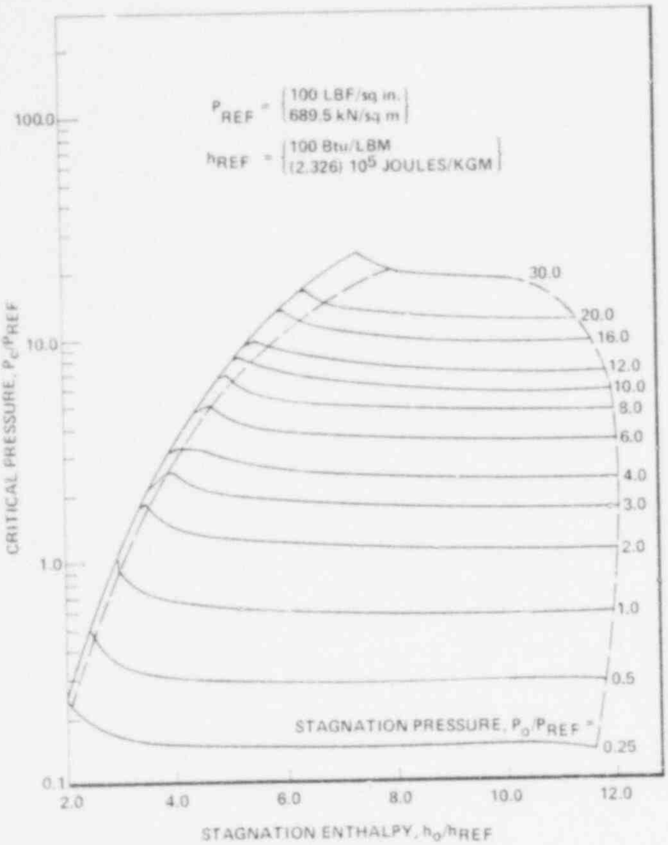

Fig.2 Critical pressure - homogeneous, equilibrium steam-water

$$\text{Mass:}\quad d[A_i(u_i+V)/v_i] + \dot{m}_{ij} - \dot{m}_{ji} = 0 \tag{9}$$

$$\text{Momentum:}\quad d[A_i(u_i+V)u_i/v_i] + \dot{m}_{ij}u_i - \dot{m}_{ji}u_j + g_c A_i dp = 0 \tag{10}$$

$$\text{Energy:}\quad d[A_i(u_i+V)h_{oi}/v_i] + \dot{m}_{ij}h_{oij} - \dot{m}_{ji}h_{oji} - A_i V dp = 0 \tag{11}$$

Stagnation enthalpies are defined by

$$h_{oi} = h_i + u_i^2/2g_c \tag{12}$$

$$h_{oij} = h_j + u_i^2/2g_c \tag{13}$$

$$h_{oji} = h_i + u_j^2/2g_c \tag{14}$$

The second law is not required for integration of the conservation equations, but it is useful later for identifying the stable range of slip ratio:

$$\text{Second law:}\quad d[A_i(u_i+V)s_i/v_i] + \dot{m}_{ij}s_j - \dot{m}_{ji}s_i \geq 0 \tag{15}$$

Next, the conservation equations for both phases are added and simplified with the substitutions,

$$u_g = v^*G \tag{16}$$

$$K = u_g/u_f \tag{17}$$

$$v^* = xv_g + (1-x)Kv_f = v^*(p,x,K) \tag{18}$$

$$A_g/A = xv_g/v^* \tag{19}$$

$$GA = u_g A_g/v_g + u_f A_f/v_f \tag{20}$$

$$A = A_g + A_f \tag{21}$$

$$x = u_g A_g/v_g GA \tag{22}$$

$$\alpha = A_g/A \tag{23}$$

$$v_m = v^*\left(x + \frac{1-x}{K}\right) = v_m(p,x,K) \tag{24}$$

$$v_e^2 = v^{*2}\left(x + \frac{1-x}{K^2}\right) = v_e^2(p,x,K) \tag{25}$$

The resulting combined equations are given by,

$$\text{Mass:}\quad d(GA) + d\left[AV\left(\frac{\alpha}{v_g} + \frac{1-\alpha}{v_f}\right)\right] = 0 \tag{26}$$

$$\text{Momentum:}\quad d(G^2Av_m) + d(VGA) + g_c A dp = 0 \tag{27}$$

$$\text{Energy:}\quad d(GAh_o) + d\left[V\left(\frac{A_f}{v_f}h_{of} + \frac{A_g}{v_g}h_{og}\right)\right] - AVdp = 0 \tag{28}$$

$$\text{Second law:}\quad d(GAs) + d\left[V\left(\frac{A_f}{v_f}s_f + \frac{A_g}{v_g}s_g\right)\right] \geq 0 \tag{29}$$

in which

$$h_o = h(p,x) + G^2v_e^2(p,x,K)/2g_c = h_o(p,x,G,K) \tag{30}$$

$$h(p,x) = xh_g + (1-x)h_f \tag{31}$$

$$s(p,x) = xs_g + (1-x)s_f \tag{32}$$

Equations (26) through (29) express differential changes across a small disturbance which moves against the flow. If conditions of equation (2) are satisfied, an appropriate interpretation for a general flow passage with variable area is that no disturbance is present. Another interpretation which applies to either a uniform area flow passage or a nozzle throat is that a disturbance does exist but is stationary (see Appendix II). For either case, imposing the conditions of equation (2) reduces equations (26) through (29) to the steady equations for slip flow [see for example, Wallis (23) or Lahey (22)]:

$$\text{Mass:}\quad d(GA) = 0 \tag{33}$$

$$\text{Momentum:}\quad d\left[G^2Av_m(p,x,K)\right] + g_c A dp = 0 \tag{34}$$

$$\text{Energy:}\quad d[GAh_o(p,x,G,K)] = 0 \tag{35}$$

597 171

$$\text{Second law:} \quad d[GAs(p,x)] \geq 0 \tag{36}$$

Suppose that steady flow occurs, and that the critical flow condition of equation (1) is satisfied either at a nozzle throat or in a uniform area section. Expansion of equations (26) through (29) shows that if equation (1) is satisfied, conditions of equation (2) also would be satisfied if a disturbance occurred. It follows that - even in slip flow - the sonic and critical flow states can occur simultaneously.

It is desirable to integrate the flow properties from some known state, say stagnation conditions in the vessel, to the critical flow state of equation (1). If p is considered independent, equations (26), (27), and (28) include four dependent variables, namely G, A, x, and K. Obviously one more equation is required for integration. Ogasawara (26) and Giot and Fritte (27) showed that momentum or energy conservation for either phase is sufficient for one more independent equation. However, an approach which involves entropy production is equivalent, and is employed in this study. The Gibbs equation for either phase,

$$T ds_i = dh_i - v_i dp \tag{37}$$

and the Clapeyron equation,

$$T s_{fg} = h_{fg} \tag{38}$$

were employed with equations (9) through (14), (20), (31), and (32) to express the entropy differential as,

$$ds(p,x) = \frac{1}{T}\left(\frac{\dot{m}_{fg} + \dot{m}_{gf}}{(dp)GA}\right)\left(\frac{u_g - u_f}{2g_c}\right)^2 dp$$

$$= \theta(p,x,G,K)dp \tag{39}$$

The vaporization and condensation rates per unit pressure reduction for phase equilibrium are given by

$$\frac{\dot{m}_{fg}}{(dp)GA} = \frac{T}{h_{fg}} \; \frac{\left[-(1-x)s_f' + Zxs_g'\right]}{1 + Z^2} \tag{40}$$

$$\frac{\dot{m}_{gf}}{(dp)GA} = \frac{T}{h_{fg}} \; \frac{\left[xs_g' + Z(1-x)s_f'\right]}{1 + Z^2} \tag{41}$$

where

$$Z = \frac{(u_g - u_f)^2}{2g_c h_{fg}} \tag{42}$$

Equation (39) displays the entropy production due to phase change with relative motion between the phases, discussed by Wallis (23). Although interfacial friction is neglected, the entropy-producing mechanism is an effective shear stress, generated by momentum transfer between the phases which are moving at unequal velocities. Equation (39) provides one more independent equation for use with equations (26), (27), and (28).

Equation (26) is useful in eliminating flow area, A, from (27), (28), and (39), which can be written in matrix form as

$$\begin{bmatrix} a_{11} & a_{12} & a_{13} \\ a_{21} & a_{22} & a_{23} \\ a_{31} & a_{32} & a_{33} \end{bmatrix} \begin{bmatrix} dG \\ dx \\ dK \end{bmatrix} = \begin{bmatrix} b_1 \\ b_2 \\ b_3 \end{bmatrix} dp \tag{43}$$

where

$$\left.\begin{aligned}
a_{11} &= \frac{G}{g_c} v_m & a_{12} &= \frac{G^2}{g_c}\frac{\partial v_m}{\partial x} \\
a_{13} &= \frac{G^2}{g_c}\frac{\partial v_m}{\partial K} & a_{21} &= \frac{G}{g_c} v_e^2 \\
a_{22} &= \frac{G^2}{2g_c}\frac{\partial v_e^2}{\partial x} + \frac{\partial h}{\partial x} & a_{23} &= \frac{G^2}{2g_c}\frac{\partial v_e^2}{\partial K} \\
a_{31} &= 0 & a_{32} &= \frac{\partial s}{\partial x} \\
a_{33} &= 0 & b_1 &= -\left(\frac{G^2}{g_c}\frac{\partial v_m}{\partial p} + 1\right) \\
b_2 &= -\left(\frac{G^2}{2g_c}\frac{\partial v_e^2}{\partial p} + \frac{\partial h}{\partial p}\right) & b_3 &= -\left(\frac{\partial s}{\partial p} - \theta\right)
\end{aligned}\right\} \tag{44}$$

Equation (43) can be integrated from stagnation to the point where equation (1) is satisfied. For this procedure, a starting value of K is required. Equations (9) and (10) show that at the stagnation limit where G approaches zero, the value of K must be $(v_g/v_f)^{1/2}$. Resulting values of the slip critical mass flux always are higher than the homogeneous flow values, and are within about 6 percent of earlier results presented by Moody (13), which are based on mass and energy conservation, and the assumption of isentropic flow. However, it is seen from equation (39) that isentropic flow cannot occur unless there is either no phase change or relative motion between the phases.

Homogeneous critical flow is expected to control mass flux in the pipe entrance region during blowdown. Therefore, it is necessary to consider slip critical flow in terms of local properties. Applying equation (1) to (43), the critical flow condition becomes,

$$\frac{dG}{dp} = \begin{vmatrix} b_1 & a_{12} & a_{13} \\ b_2 & a_{22} & a_{23} \\ b_3 & a_{32} & a_{33} \end{vmatrix} = 0 \tag{45}$$

which results in a solution for the slip critical mass flux $G_c(p,x,K)$.

STABLE RANGE OF SLIP RATIO

A reasonable lower limit for K is 1.0 for phases traveling at equal speeds. An upper limit can be determined from the second law. Eliminating GA from equations (33) and (36) and combining with (39), it follows that

$$ds = \theta dp \geq 0 \tag{46}$$

597 172

From equations (43) and (46), it can be shown that

$$\theta\frac{dp}{dK}\,dK = \theta\,\frac{\begin{vmatrix} a_{11} & a_{12} & a_{13} \\ a_{21} & a_{22} & a_{23} \\ a_{31} & a_{32} & a_{33} \end{vmatrix}}{\begin{vmatrix} a_{11} & a_{12} & b_1 \\ a_{21} & a_{22} & b_2 \\ a_{31} & a_{32} & b_3 \end{vmatrix}}\,dK \geq 0 \qquad (47)$$

A detailed study of the above inequality shows that for fixed values of p, x, and G, K will always be changing in a direction which makes

$$\begin{vmatrix} a_{11} & a_{12} & b_1 \\ a_{21} & a_{22} & b_2 \\ a_{31} & a_{32} & b_3 \end{vmatrix} = 0 \qquad (48)$$

The value of K which satisfies equation (48) is considered the stable value, and also the upper limit. Simultaneous solutions of equations (45) and (48) were obtained numerically to express the critical mass flux and the maximum slip ratio in terms of local pressure and quality. Results are graphed in Figure 3. Also shown are results for a slip ratio of 1.0.

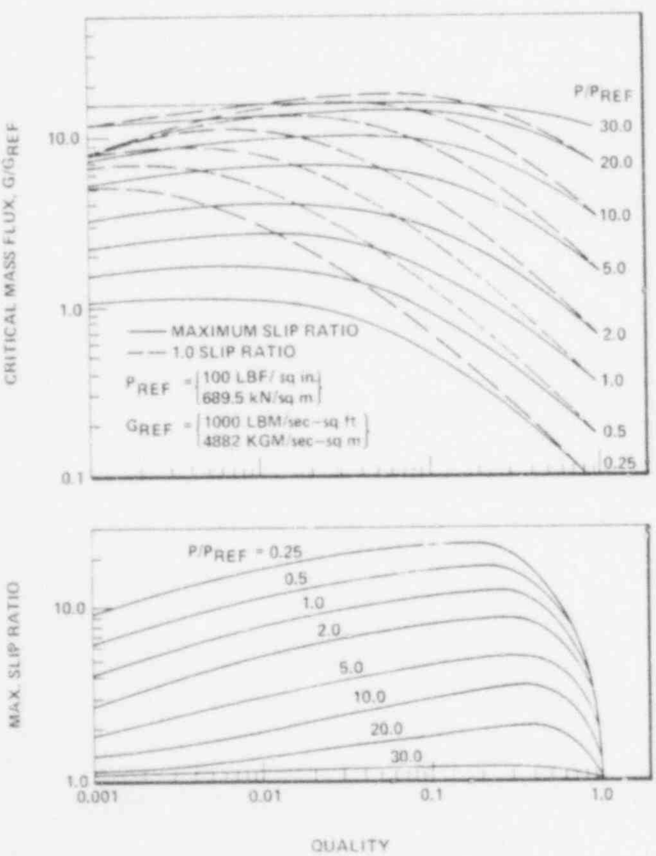

Fig.3 Critical flow states - slip model

COMPARISONS WITH DATA

Equilibrium blowdown data is employed in this section to show that two-phase blowdown rates are controlled by homogeneous choking near the pipe entrance, followed by a second choked condition for slip flow near the exit.

Two Critical Flow States During Blowdown

Figure 4 presents blowdown mass flux and pipe exit pressure data of Sozzi and Sutherland (7) for 1.27 cm (0.5 in.) i.d. pipes of various lengths and vessel stagnation pressures between 65 and 70 atmospheres. The data is graphed as a function of stagnation quality, defined as

$$x_o = \frac{v - v_f(p_o)}{v_{fg}(p_o)} \qquad (49)$$

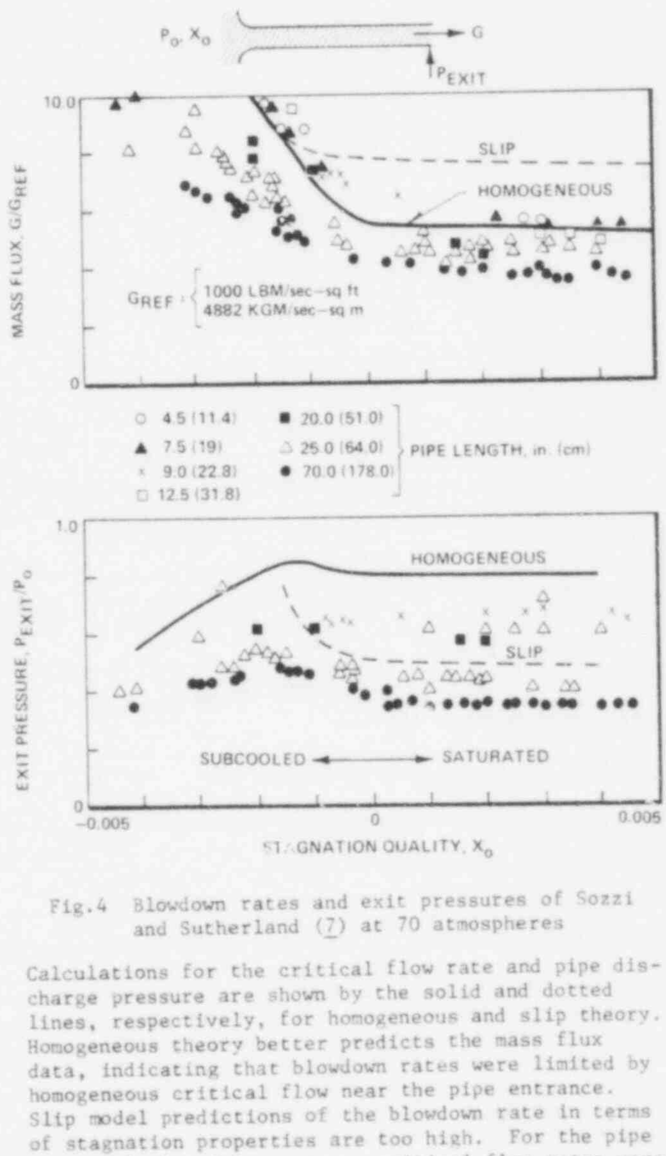

Fig.4 Blowdown rates and exit pressures of Sozzi and Sutherland (7) at 70 atmospheres

Calculations for the critical flow rate and pipe discharge pressure are shown by the solid and dotted lines, respectively, for homogeneous and slip theory. Homogeneous theory better predicts the mass flux data, indicating that blowdown rates were limited by homogeneous critical flow near the pipe entrance. Slip model predictions of the blowdown rate in terms of stagnation properties are too high. For the pipe exit, calculated homogeneous critical flow rates were employed in the slip model to predict pipe exit pressures from equations (45) and (48). The slip theory prediction better represents exit pressure data. A consistent interpretation of Figure 4 is that blowdown rates are limited by homogeneous equilibrium

597 173

critical flow near the pipe entrance, and a second critical flow state occurs at the pipe exit which corresponds to a slip flow pattern.

Saturated Water Blowdown

Figure 5 shows the blowdown mass flux obtained by different workers for saturated water at various stagnation pressures. Uchida (24), Fauske (19), Henry (6), and Sozzi and Sutherland (7) employed uniform pipes from 0.4 to 1.3 cm (0.16 to 0.513 in.) i.d. Allemann (14) conducted vessel blowdowns through pipes up to 17.3 cm (6.8 in.) i.d. Data is shown only for pipes 10 cm (4 in.) or longer so that the flow rates are close to equilibrium. The solid curve shows critical mass flux calculated from homogeneous equilibrium theory. Agreement is sufficiently close to verify that the homogeneous model predicts saturated water blowdown rates for given vessel pressures. This supports an earlier conclusion of Simon (21).

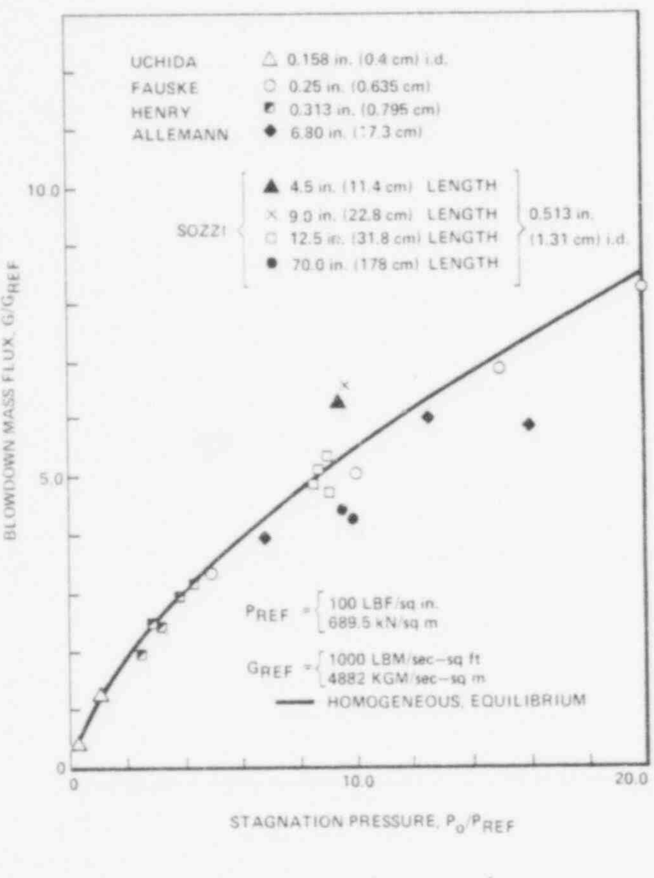

Fig.5 Blowdown rate of saturated water

Calculated homogeneous critical mass flows were compared with pipe blowdown rates of Moody (15). Results showed that when the pipe friction parameter, fL/D, is greater than about 3.0, saturated water discharge rates are limited by friction and choking at the pipe exit, and therefore are less than values determined by homogeneous critical flow at the entrance.

Subcooled and Saturated Blowdown

Figure 6 presents the blowdown mass flux data of Henry (6) for steam-water discharge through a 0.9 m (3 ft) long, 0.8 cm (0.313 in.) i.d. pipe. Static pressure taps were located on the pipe to give a description of the pressure profile. Stagnation pressure was estimated from the most upstream pressure tap, located 76 cm (30 in.) from the pipe exit. Blowdown rates calculated from homogeneous theory are shown by solid lines. Close agreement was obtained showing that for both saturated and subcooled stagnation states, blowdown rates are limited by homogeneous choking near the pipe entrance.

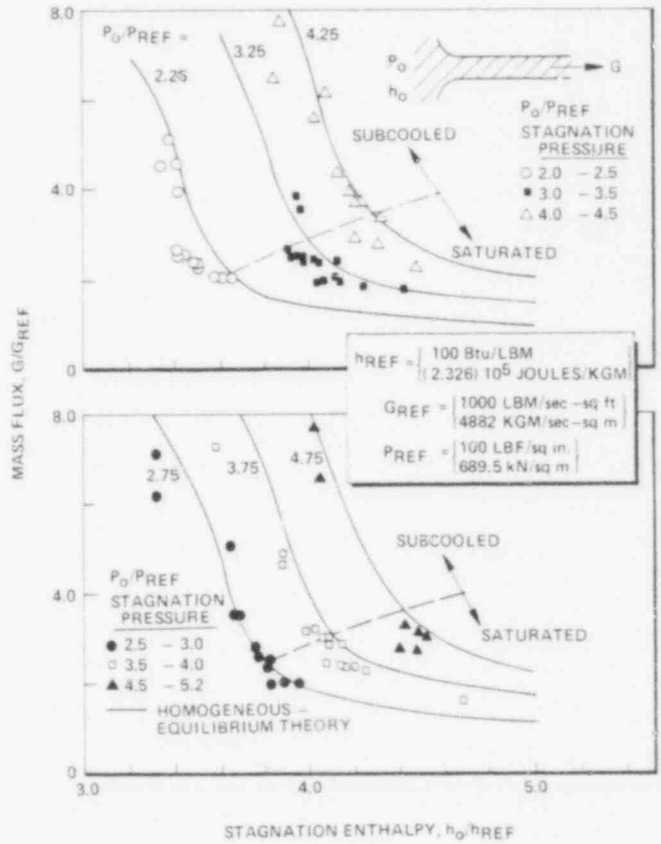

Fig.6 Blowdown rates of Henry (6)

Figure 7 shows pipe exit pressures for the same data of Henry (6) presented in Figure 6. Blowdown rates calculated from the homogeneous model in terms of stagnation properties were employed to determine pipe exit pressure from the slip model. Calculated results compare sufficiently well to verify the existence of a choked slip condition at the exit.

Blowdown Flow and Pipe Discharge Properties

Data for steam-water blowdowns in terms of pipe exit properties has been obtained by numerous workers and reported in References 1 through 5. In addition, data of Henry (6), and Sozzi and Sutherland (7), already presented in Figures 4, 6, and 7 in terms of stagnation properties, includes the pipe exit properties. The pipe exit data is presented in Figure 8 as a function of static pressure and quality. All data is for flow passages longer than 10 cm (4 in.) so that equilibrium is assured. The solid curves were calculated from the slip model at the maximum slip ratio. Agreement further indicates that near the pipe exit, a choked slip flow occurs.

597 174

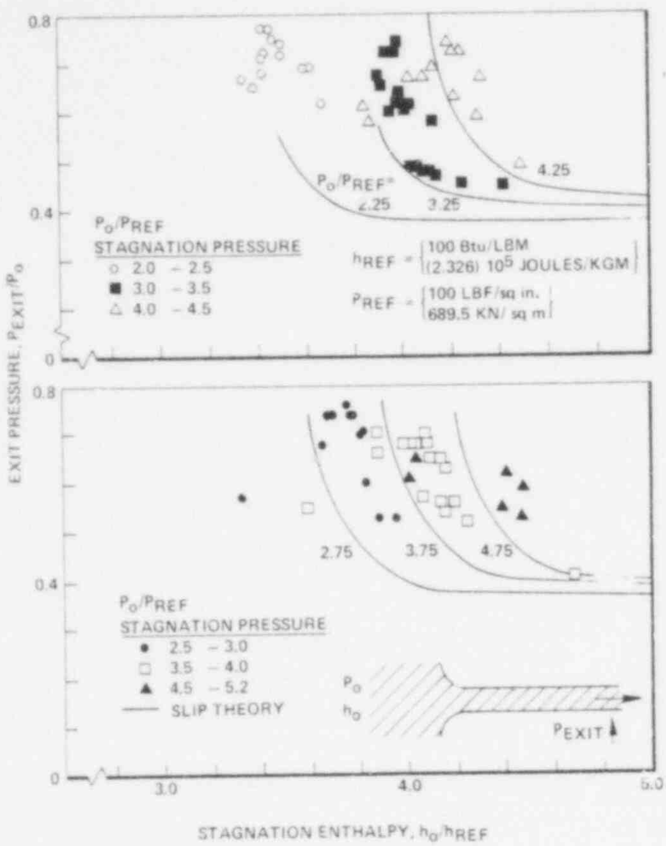

Fig.7 Pipe exit pressures of Henry (6)

Low quality data of Henry (6) is shown in Figure 9. For quality below 0.02, predictions with the slip model at the maximum slip ratio are too low, and the data appear to be bounded by a slip ratio of 1.0 and the maximum value.

CONCLUSIONS

The following conclusions from this study are restricted to flow passages sufficiently long for saturated equilibrium to be closely approached between the liquid and vapor. For steam-water flows, the flow length should be 10 cm (4 in.) or longer.

1 During two-phase blowdown from vessels, flow pattern in the pipe entrance is a homogeneous mixture of vapor bubbles in liquid.

2 Two-phase blowdown rates from vessels are predicted by the homogeneous, equilibrium, choked state in terms of stagnation properties in the vessel (Fig.1).

3 Downstream from the pipe entrance, the two-phase blowdown probably tends toward a slip flow pattern.

4 Pipe discharge rates at the exit are predicted by the choked state of a slip flow model.

5 The pipe exit choked flow state does not influence homogeneous choking at the entrance for pipe friction parameters of $fL/D < 3.0$.

6 For values of the friction parameter $fL/D > 3.0$, pipe entrance flow will unchoke, and blowdown rates will be less than that predicted by homogeneous choking in terms of vessel stagnation properties.

7 The slip ratio in an equilibrium choked flow is bounded by 1.0 and an upper limit determined by second law requirements.

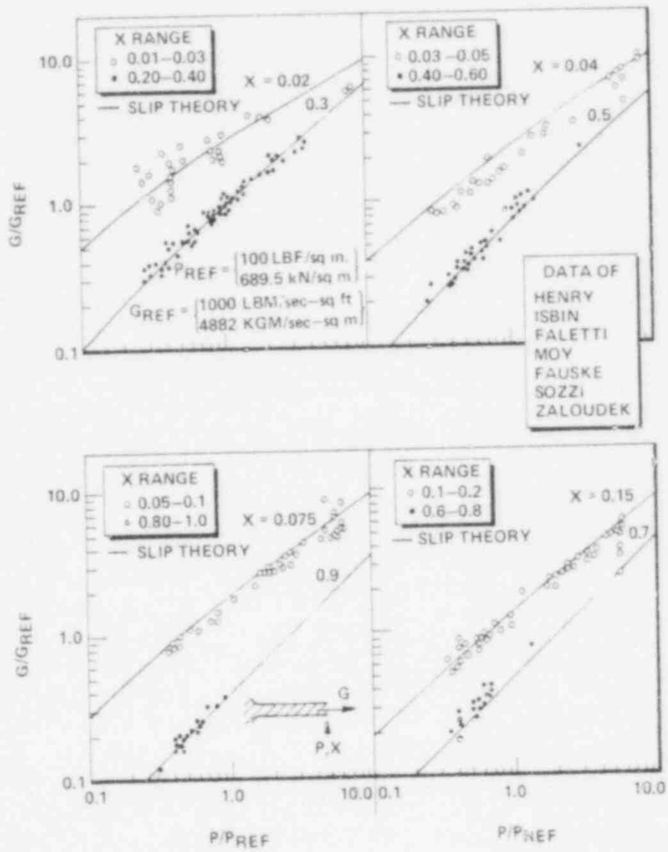

Fig.8 Critical flow properties at pipe exit

REFERENCES

1 Faletti, D. W., "Two-Phase Critical Flow of Steam/Water Mixtures," Dissertation, 1959, University of Washington.

2 Moy, J. E., "Critical Discharges of Steam/Water Mixtures," M.S. Thesis, 1955, University of Minnesota.

3 Isbin, H. S., Moy, J. E., and DaCruz, A. J. R., "Two Phase Steam/Water Critical Flow," Trans. AIChE, Vol. 3, No. 3, 1957, pp. 361-365.

4 Fauske, H. K., "Contribution to the Theory of Two-Phase, One-Component Critical Flow," ANL-6633, 1962, Argonne National Laboratory, LeMont, Ill.

5 Zaloudek, F. R., "The Low Pressure Critical Discharge of Steam/Water Mixtures from Pipes," HW-68934 Rev., 1961, Hanford Atomic Products Operation, Richland, Wash.

6 Henry, R. E., "An Experimental Study of Low-Quality, Steam-Water Critical Flow at Moderate Pressures," ANL-7740, 1970, Argonne National Laboratory, LeMont, Ill.

7 Sozzi, G. L., and Sutherland, W. A., "Critical Flow of Saturated and Subcooled Water at High Pressure," NEDO-13418, May 1975, General Electric Company, San Jose, Calif.

8 Henry, R. E., "A Study of One- and Two-Component, Two-Phase Critical Flows at Low Qualities," ANL-7430, 1968, Argonne National Laboratory, LeMont, Ill.

597 175

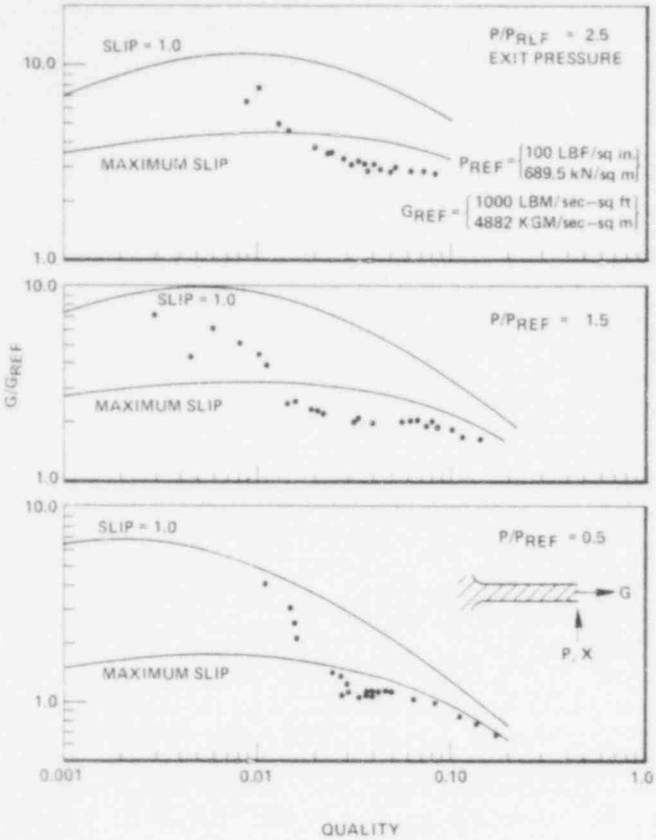

Fig.9 Low quality data of Henry (6)

9 Henry, R. E., "The Two-Phase Critical Discharge of Initially Saturated or Subcooled Liquid," Nuclear Science and Engineering, Vol. 41, 1970, pp. 336-342.

10 Edwards, A. R., "Conduction Controlled Flashing of a Fluid, and the Prediction of Critical Flow Rates in a One-Dimensional System," AHSB(S)R-147, 1968, U.K.A.E.A., A.W.R.E., Foulness Island, South End on Sea, Essex, England.

11 Boure', J. A., "Two-Phase Flows with Application to Nuclear Reactor Design Problems," vonKarman Institute for Fluid Dynamics Lecture Series, Dec. 9-13, 1974, Service des Transferts Thermiques, Centre d'Etudes Nucleaires de Grenoble, France.

12 Levy, S., "Prediction of Two-Phase Critical Flow Rate," Trans. ASME, JHT, Ser. C, Vol. 87, No. 1, 1965, p. 53.

13 Moody, F. J., "Maximum Flow Rate of a Single Component, Two-Phase Mixture," Trans. ASME, JHT, Ser. C, Vol. 87, No. 1, 1965, p. 134.

14 Allemann, R. T., et al., "Experimental High Enthalpy Water Blowdown from a Simple Vessel Through a Bottom Outlet," BNWL-1411, 1970, Battelle Northwest Laboratory, Richland, Wash.

15 Moody, F. J., "Maximum Two-Phase Vessel Blowdown from Pipes," Trans. ASME, JHT, Ser. C, Vol. 88, 1966, p. 285.

16 Edwards, A. R., and O'Brien, T. P., "Studies of Phenomena Connected with the Depressurization of Water Reactors," Journal of the British Nuclear Energy Society, Vol. 9, 1970.

17 Zaker, T. A., and Wiedermann, A. H., "Water Depressurization Studies," IITRI-578-p-21-26, 1966, Illinois Institute of Technology, Chicago, Ill.

18 Gallagher, E. V., "Water Decompression Experiments and Analysis for Blowdown of Nuclear Reactors," IITRI-578-p-21-39, 1970, Illinois Institute of Technology, Chicago, Ill.

19 Fauske, H. K., "The Discharge of Saturated Water Through Tubes," Symposium Series 61, Chemical Engineering Progress, 1965, p. 210.

20 Uchida, H., and Nariai, H., "Discharge of Saturated Water Through Pipes and Orifices," Proceedings of the Third International Heat Transfer Conference, Vol. 5, 1966.

21 Simon, U., "Blowdown Flow Rates of Initially Saturated Water," Paper presented at the European Two-Phase Flow Meeting, Risø, Denmark, June 1971.

22 Lahey, R. T., "Two-Phase Flow in Boiling Water Nuclear Reactors," NEDO-13388, July 1974, General Electric Company, San Jose, Calif.

23 Wallis, G. B., One Dimensional Two-Phase Flow, McGraw-Hill, New York, 1969.

24 Kober, K. J., et al., "Untersuchungen zur Simulation der Drukentlastung von Siedwasserreactoren," Forschungsauftrag Nr. RS 16, 1968, Battelle Institute, Frankfurt, Germany.

25 Henry, R. E., Fauske, H. K., and McComas, S. T., "Two-Phase Critical Flow at Low Qualities, Part 1: Experimental," Nuclear Science and Engineering, Vol. 41, 1970, pp. 79-91.

26 Ogasawara, H., "A Theoretical Prediction of Two-Phase Critical Flow," Japan Society of Mechanical Engineers Bulletin, Vol. 10, No. 38, 1967.

27 Giot, M., and Fritte, A., "Two-Phase, Two- and One-Component Critical Flows with the Variable Slip Model," Progress in Heat and Mass Transfer, Vol. 6, Pergamon Press, New York, 1972, p. 651.

APPENDIX I CONSERVATION EQUATIONS FOR MOVING DISTURBANCE

Figure A-1 shows two separated phases, designated i and j, undergoing one-dimensional flow to the right in a flow passage of variable area, with a disturbance moving to the left at velocity V. Wall and interface friction are assumed to be negligible.

Static pressure is uniform through each phase at any flow cross section. Moving with the disturbance in phase i is a control volume which is sufficiently thin that mass, momentum, and energy storage inside can be neglected. Mass conservation for the control volume is written as

$$d\dot{m}_i + \dot{m}_{ij} - \dot{m}_{ji} = 0 \qquad (50)$$

where $\dot{m}_i$ is the mass flow rate relative to the control volume, given by

$$\dot{m}_i = A_i(u_i + V)/v_i \qquad (51)$$

Equations (50) and (51) can be combined to give equation (9).

Momentum conservation is written assuming that mass rate $\dot{m}_{ij}$ leaves the control volume with velocity u_i and $\dot{m}_{ji}$ enters with velocity u_j:

$$d(\dot{m}_i u_i) + \dot{m}_{ij}u_i - \dot{m}_{ji}u_j + g_c A_i dp = 0 \qquad (52)$$

Equations (51) and (52) yield (10).

It is assumed that mass rate $\dot{m}_{ij}$ leaves the control volume as phase j with static enthalpy h_j but with velocity u_i, and that $\dot{m}_{ji}$ enters as phase i with h_i and u_j. Appropriate stagnation enthalpies are given by equations (12), (13), and (14). Work is done as the control volume moves at rates pA_iV,

597 176

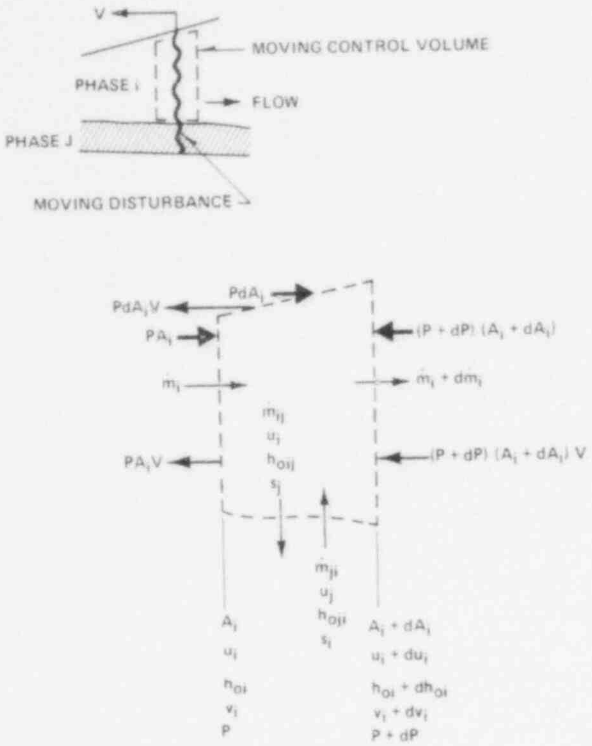

Fig.A-1 Control volume moving with disturbance

$pVdA_i$, and $(p + dp)(A_i + dA_i)V$. Therefore, energy conservation for the moving control volume is written as

$$d(\dot{m}_i h_{oi}) + \dot{m}_{ij} h_{oij} - \dot{m}_{ji} h_{oji} - A_i V dp = 0 \tag{53}$$

Equations (51) and (53) yield equation (11).

Finally, mass rate $\dot{m}_{ij}$ leaves the control volume at specific entropy s_j, and $\dot{m}_{ji}$ enters at s_i. Therefore, the second law is written as

$$d(\dot{m}_i s_i) + \dot{m}_{ij} s_j - \dot{m}_{ji} s_i \geq 0 \tag{54}$$

Equations (51) and (54) yield (15).

APPENDIX II SIMULTANEOUS CRITICAL FLOW AND SONIC STATES

For the critical flow state, equation (26) is expanded, and the condition of equation (1) is imposed to give

$$GdA + AVd\left(\frac{\alpha}{v_g} + \frac{1-\alpha}{v_f}\right) + \left(\frac{\alpha}{v_g} + \frac{1-\alpha}{v_f}\right)(AdV + VdA) = 0 \tag{55}$$

If the sonic state, given by conditions of equation (2) is to apply simultaneously with the critical flow state, equation (55) requires that $dA = 0$. It follows that one-dimensional two-phase critical flow and the sonic states can occur simultaneously in a uniform area flow passage or in a nozzle throat. If *only* the sonic conditions of equation (2) are imposed, the expanded form of equations (26) through (29) reduce to equations (33) through (36), which are identical to the steady-flow equations in a flow passage of variable area. Therefore, when the steady-flow equations satisfy the critical-flow condition of equation (1) in a section where $dA = 0$, the sonic and critical flow states occur simultaneously.

597 177

SUPPLEMENTARY INFORMATION

NRC request for this information was contained in a letter from D. G. Eisenhut (NRC) to L. J. Sobon (GE) dated August 29, 1977

GE response with the following information was provided in a letter from L. J. Sobon (GE) to D. G. Eisenhut (NRC) dated November 8, 1977

597 178

REPLY TO NRC REQUEST
FOR ADDITIONAL INFORMATION ON NEDO 21052

SECTION I. SUMMARY POINTS OF NEDO-21052

The following summary of NEDO-21052 will be helpful in the discussion which presents additional information requested by the NRC.

Point 1. Results apply to cases where two-phase saturated equilibrium is closely approached.

Point 2. Data indicates that saturated equilibrium is closely approached during mixture travel of approximately 10 cm into the discharging flow passage.

Point 3. Two choked flow conditions can occur in a blowdown flow passage. One choked condition occurs near the entrance, and another choked condition at the exit. See Figure AA.

Point 4. Bulk boiling of fluid particles undergoing rapid depressurization in the pipe entrance region first produces a homogeneous flow pattern of vapor bubbles in liquid. Therefore, equilibrium choked flow rates are limited by the homogeneous equlibrium model (HEM) near the entrance region. Once in the flow passage, decompression of a fluid particle is slower and a slip flow pattern forms, leading to a second slip-choked condition at the exit.

Point 5. The entrance choked condition is predicted by the HEM in a form which relates vessel pressure P_o, entrance stagnation enthalpy h_o, and choked mass flux G_c. The flow rate proceeding through the passage is limited by entrance homogeneous choking.

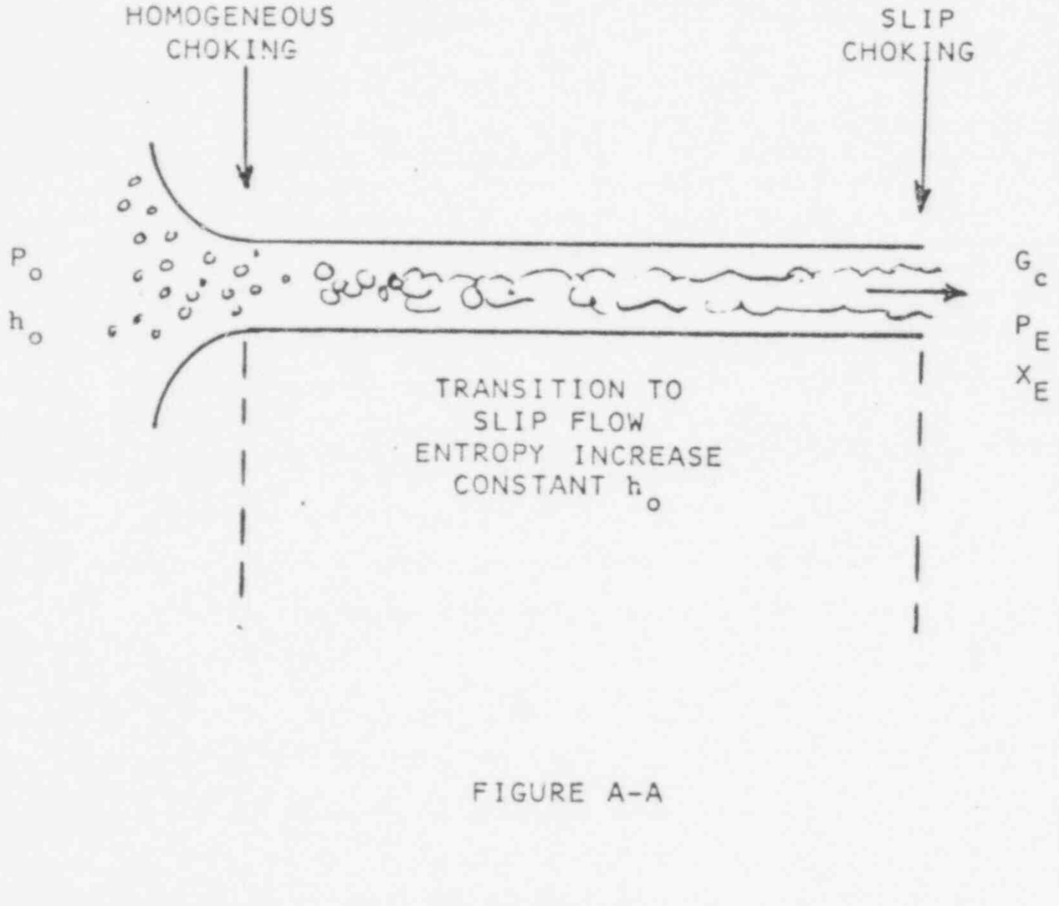
HOMOGENEOUS
CHOKING
SLIP
CHOKING
P_o
h_o
G_c
P_E
X_E
TRANSITION TO
SLIP FLOW
ENTROPY INCREASE
CONSTANT h_o

FIGURE A-A

Point 6. The exit flow rate already is determined by entrance choking. Some degree of phase separation occurs in the flow passage between entrance and exit. The discharge condition corresponds to a choked slip equilibrium model (SEM) for which G_c and h_o are determined from entrance conditions. Exit static pressure P_e adjusts to accommodate G_c and h_o (or equivalently the exit quality x_e) for the SEM choked flow rate.

Point 7. Most of the early equilibrium choked flow data is based on discharge exit properties, best correlating P_e, x_e, and G_c at the exit by a SEM.

Point 8. Equilibrium data in terms of vessel properties is best correlated by the HEM.

Point 9. A counterpart of the two choked states in two-phase flow is found in gas dynamics. The restriction of gas flow by a nozzle in which the throat Mach number is 1.0, limits mass flow in terms of reservoir properties.

However, downstream shocking and pipe friction may produce an exit condition also at Mach 1.0, with the same flow rate and stagnation enthalpy occuring at the nozzle, but at pressure, density, and temperature different from nozzle properties.

Point 10. It is not possible to take choked flow data presented in terms of discharge properties and directly obtain stagnation properties appropriate for upstream homogeneous choking. The reason is that although stagnation enthalpies at entrance and exit are equal, the entropy change associated with transition from homogeneous to slip flow reduces the stagnation pressure in the direction of flow. A counterpart in gas dynamics would be to take discharge choked flow properties and attempt to predict entrance stagnation properties without knowing the area ratio of an upstream Mach 1.0 nozzle which limits the flow rate.

SECTION II. RESPONSE TO NRC REQUESTS

REQUEST 1

Critical flow measurements have been made by a number of experimenters. In several cases the data have been compared with the predictions of the homogeneous equilibrium model (HEM). In each of the references listed below the experimentally determined critical flows were found to exceed the values predicted by the HEM model.

These conclusions indicate that use of HEM to predict break flow is not conservative for containment analysis. For each of the following data sets provide a comparison of the experimental critical flows with the homogeneous equilibrium model in NEDO-21052 and justify any differences in your conclusions with those of the author.

a. M. W. Benjamin and J. G. Miller, "The Flow of Saturated Water Through Throttling Orifices," Trans. ASME, Vol. 63, p. 419 (1941).

b. D. W. Faletti and R. W. Moulton, "Two-Phase Critical Flow of Stream-Water Mixtures," AIChE Journal, Vol. 9, p. 247 (1963).

c. F. R. Zaloudek, "The Critical Flow of Hot Water Through Short Tubes," HW-77594, Hanford Works, (1963).

   F. R. Zaloudek, "Steam-Water Critical Flow From High Pressure Systems," Interim Report, HW-80535, Hanford Works, (1964).

d. H. K. Fauske, "Contribution to the Theory of Two-Phase, One-Component Critical Flow," AEC Report, ANL-6633, (October 1962).

e. R. E. Henry, "A Study of One- and Two-Component, Two-Phase Critical Flows at Low Qualities," ANL-7430, Argonne National Laboratory, (1968). R. E. Henry, H. K. Fauske, and S. T. McComas, "Two-Phase Critical Flow at Low Qualities," Nuclear Science and Engineering, Vol. 41, pp. 79-98, (1970).

f. E. S. Starkman, V. E. Schrock, K. F. Neusen, and D. J. Maneely, "Expansion of a Very Low Quality Two-Phase Fluid through a Convergent-Divergent Nozzle,' Journal of Basic Engineering, Trans, ASME, pp. 247-256, (June 1964).

RESPONSE TO REQUEST 1

Responses to this request, given below, refer to each individual reference by the alphabetical designation above.

(a) An orifice does not represent a flow passage long enough to assure phase equilibrium (Summary Points 1 & 2 of Section I). The models of NEDO-21052 are restricted to equilibrium states, and therefore permit no meaningful comparison with orifice flows. In the limit, an orifice would represent a flow length of zero, which clearly results in too short a transit time for nucleation and bubble growth to achieve phase equilibrium.

(b) Faletti's data was obtained in annular flow passages which were long enough to assure phase equilibrium. Figure 8 of NEDO-21052 shows that this data is well predicted by the SEM in terms of exit choked properties. However, upstream stagnation properties were not presented and a meaningful comparison with the HEM cannot be made (Summary Points 1 & 2 of Section I).

(c) A meaningful comparison cannot be made with data of Zaloudek for short flow passages of 3.0 inches and less (Points 1 & 2 of Section I). However, Zaloudek's data for longer flow passages is well predicted by the SEM in Figure 8 of NEDO-21052.

(d) Fauske's data was obtained in test sections long enough to assure phase equilibrium, and is included in Figure 8 of NEDO-21052. The data is seen to be predicted by the SEM as

597 183

expected since measurements yielded exit properties. This data in terms of exit properties represents a slip-choked condition, and should not correlate with the HEM. Additional work of Fauske reported in Ref. 19 of NEDO-21052, which gives stagnation pressures, is predicted well by the HEM.

(e) Henry's reference ANL 7430 presents data similar to that given in ANL 7740, which is shown in Figures 6 and 7 of NEDO-21052, and strongly supports the existence of entrance homogeneous and exit slip choked conditions.

The references of Henry, Fauske, and McComas deals with two-dimensional rapid expansion effects at the exit. Their study incorporates data reported elsewhere, and leads to the conclusion that although discharge slip ratios are less than required for annular flow, some degree of slip occurred, which is consistent with the description of NEDO-21052. No further comparisons were made with material in these references.

(f) The data of Starkman, et.al. was based on short converging-diverging flow nozzles, and therefore is not appropriate for comparison with equilibrium models (Points 1 & 2 of Section I).

REQUEST 2

A comparison of various critical flow data in the following reference including those data of G. Sozzi* demonstrates that the HEM model under-predicts experimental data. Justify the differences between the conclusions in NEDO-21052 and those of the authors.

K. H. Ardron and R. A. Furness, "A Study of the Critical Flow Models Used in Reactor Blowdown Analysis," Nuclear Engineering and Design 39, (1976), p. 257-266.

---

* Sozzi, G. L., and Sutherland, W. A., "Critical Flow of Saturated and Subcooled Water at High Pressure," NEDO-13418, May 1975.

597 184

RESPONSE TO REQUEST 2

The following responses pertain to figures contained in the reference by Ardron and Furness.

The data of Maneely and Friedrich in Figure 2 is for flow passages too short to assure equilibrium (Points 1& 2 of Section I). Therefore, no valid comparison can be made with equilibrium models. The data of Fauske and Faletti in Figure 2 was not presented in the original references in terms of stagnation conditions. The procedure employed by Ardron and Furness to obtain stagnation properties is not described, and leaves the results of Figure 2 open to question (Point 10 of Section I). The same data of Faletti and Fauske compares favorably with the SEM in Figure 8 of NEDO-21052 in terms of the published discharge properties.

Data in Figure 3 is for flow passages too short to achieve phase equlibrium, and should not be compared with either the HEM in terms of stagnation properties or the SEM in terms of discharge properties (Points 1 & 2 of Section I).

Figure 4 at 62 bars includes some data from flow passages too short for equilibrium, i.e. less than about 10 cm, for which no valid comparison can be made with equilibrium models (Points 1& 2 of Section I). The remaining data of Sozzi and Sutherland falls close to the HEM curve. It appears that the Sozzi-Sutherland experimental points selected for this comparison are from the upper error band of their collected data since additional data from the same series of tests, presented in Figure 4 of NEDO-21052, shows a distribution above and below the HEM.

Figure 5 for saturated water blowdown contains only a few data points of Fauske at L/D = 40 with D = 6 mm and of the apparently upper error band data of Sozzi and Sutherland at L/D = 18 and 29 with D = 12.7 mm, most of which lie close to the HEM. Figure 5 of NEDO-21052 shows most of the same applicable data plus some additional points of Allemann for a 6.8 inch pipe, which lie below the HEM.

Although it is a minor observation, it appears that the theoretical HEM curves shown by Ardron and Furness are somewhat lower than those calculated using the 1967 ASME Steam Tables, used in Ref. 1. Differences are perhaps 10 percent, but it does cause more of the data to lie below the HEM curve than is indicated by their graphs.

REQUEST 3

Semi-scale tests discussed in TREE-NUREG-1006 have produced transient critical flow data that are in general agreement with the HEM model for two-phase flow but are in excess of HEM for saturated and subcooled flows. Provide a comparison of the HEM model discussed in NEDO-21052 with the Semi-scale test data and justify the differences in your conclusion with those of the author.

D. G. Hall, "A Study of Critical Flow Prediction for Semi-scale Mod-1 Loss-of-Coolant Accident Experiments," TREE-NUREG-1006, Idaho National Engineering Laboratory, December 1976.

RESPONSE TO REQUEST 3

The HEM of NEDO-21052 should not be compared with the semi-scale tests discussed in TREE-NUREG-1006, which were based on flow nozzles too short to permit phase equlibrium (Points 1 & 2 of Section I). The semi-scale tests use a "Henry" nozzle for limiting the blowdown flow rate. This nozzle has a relatively short throat length, less than 1.0 inch and is known to produce non-equilibrium phase change. Henry* "calibrated" the non-equlibrium effects by an "N-Factor" to account for differences between equilibrium and non-equilibrium flashing. It is interesting to note that semi-scale has recently replaced the Henry nozzle with one of slightly longer throat length, about 3.0 inch.** This new nozzle is

---

* Henry, R. R., and Fauske, H. K., "The Two-Phase Critical Flow of One Component Mixtures in Nozzles, Orifices, and Short Tubes," ASME Paper No. 70-WA/H7-5.

** TREE-NUREG-1118, Aug. 1977

scaled from the LOFT counterpart. Although these nozzles (Henry and LOFT counterpart) had the same flow area, the longer length nozzle produced significantly lower blowdown flow rates.

REQUEST 4

Page 2 of NEDO-21052 states that for pipe lengths greater than 10 cm, the discharge rate is unaffected by further increases in pipe length. This conclusion is inconsistent with the data of Sozzi* in Figure 5 which indicate the flow is greater for a 9-inch pipe length than for a 4.5-inch length or a 12.5-inch length. Discuss the reasons for this inconsistency.

RESPONSE TO REQUEST 4

The word "unaffected" in NEDO-21052 is too strong, and would be accurate if it were revised to read "not strongly affected". Further increases of pipe length beyond approximately 10 cm show an extremely reduced effect on flow rate. The data of Sozzi and Sutherland shown in Figure 5 of NEDO-21052 is subject to a degree of uncertainty in measurement, and some scatter is expected. The collection of data presented in Figure 5 of NEDO-21052 from several investigators shows a strong trend of agreement with the HEM.

REQUEST 5

Page 3 states that steady-state flow is required upstream before HEM equation 8 can be derived. Justify the applicability of this equation for transient critical flow.

---

* Sozzi, G. L., and Sutherland, W. A., "Critical Flow of Saturated and Subcooled Water at High Pressure," NEDO-13418, May 1975.

RESPONSE TO REQUEST 5

The term "steady flow" is here regarded as "quasi-steady flow". Unsteadiness in the flow is attributed to either the initial rupture and decompression of a pipe, or the time-dependent vessel pressure reduction. The material of NEDO-21052 applies after initial pipe decompression when all propagation effects have disappeared. Instantaneous values of vessel pressure should be employed in predicting discharge rates as long as vessel decompression rate is slow relative to the residence time of a fluid particle as it travels through the pipe.

REQUEST 6

Provide the details of the mathematical solution of equation 8 used to produce the critical flows in Figure 1 and the critical pressure ratios in Figure 2.

RESPONSE TO REQUEST 6

One could obtain the partial derivative of v with respect to P at constant entropy s directly from a programmed steam table library at given values of P and quality x, then obtain corresponding stagnation enthalpy h_o and pressure P_o from additional energy and state equations. However, the procedure employed to obtain Figure 1 of Ref. 1 was based on the energy equation,

$$h_o = h + \frac{G^2 v^2}{2g_c}$$

for homogeneous flow. The above equation was written as

$$G = \sqrt{\frac{2g_c(h_o - h_f - xh_{fg})}{v_f + xv_{fg}}}$$

where $$x = \frac{s_o - s_f}{s_{fg}}$$

Beginning with stagnation properties P_o and h_o, the entropy s_o was determined from the 1967 ASME Steam Properties. Then G was calculated for successively lower pressures P until an absolute maximum of G was found numerically, which was termed GM at pressure PM. This procedure is valid for homogeneous flows, but not for slip flows. The computation is straightforward and accurate when the stagnation state is saturated. However, subcooled stagnation states sometimes lead to very sharp peaks of G which are difficult to determine accurately. However, static pressure PM at the peak G is quite distinct. It was noted that the sharp peaks in G for some subcooled stagnation states occurred at very low qualities associated with the HEM, and therefore, a frictionless liquid flow rate GBM was obtained from the Bernoulli equation for an incompressible liquid flowing from stagnation pressure to PM. The greater of GBM or GM was employed to obtain Figure 1 in NEDO-21052. Results of this procedure were verified by a number of computations giving pressures and flow rates at 1.0 psi increments to observe the actual GM and PM where the peak occurred. Discrepancies were negligible.

REQUEST 7

Provide the critical flows in Figure 1 in tabular form for subcooled and two-phase critical flows at 10% increments of stagnation quality at the following stagnation pressure in psia: 100., 200., 400., 600., 800., 1000., 1200.

597 189

RESPONSE TO REQUEST 7

The following tables provide the information requested. Stagnation qualities shown are not all at precise 10% increments, but these values were readily available from the original computations. The quality increments shown should be satisfactory. The symbols are interpreted as:

PO	=	Stagnation Pressure, Psia
HO	=	Stagnation Enthalpy, BTU/LBM
QLI	=	Stagnation Quality
GM	=	Maximum Homogeneous Mass Flux, LBM/S-Ft^2
PM	=	Pressure at Condition of Maximum Mass Flux, Psia
QLE	=	Quality at Condition of Maximum Mass Flux
GBM	=	Bernoulli mass flux based on liquid flow from stagnation pressure to PM, LBM/S-ft^2, calculated only for subcooled stagnation states.

PO = 100

STEAM DOME

HO	QLI	GM	PM	QLE
1187.1644	1.0000	206.0080	58.0000	0.96403
1151.6194	0.96000	209.9721	58.0000	0.92711
1116.0744	0.92000	214.1740	58.0000	0.89019
1080.5295	0.88000	218.6385	58.0000	0.85326
1044.9845	0.84000	223.3942	58.0000	0.81634
1009.4395	0.80000	228.4740	58.0000	0.77941
973.8946	0.76000	233.9165	58.0000	0.74249
938.3496	0.72000	239.7670	58.0000	0.70556
902.8046	0.68000	246.0791	58.0000	0.66864
867.2597	0.64000	252.9326	59.0000	0.63197
831.7147	0.60000	260.3960	59.0000	0.59496
796.1697	0.56000	268.5604	59.0000	0.55795
760.6248	0.52000	277.5427	59.0000	0.52093
725.0798	0.48000	287.4887	59.0000	0.48392
689.5348	0.44000	298.6187	60.0000	0.44673
653.9899	0.40000	311.1571	60.0000	0.40963
618.4449	0.36000	325.4134	60.0000	0.37253
582.8999	0.32000	341.8920	61.0000	0.33499
547.3550	0.28000	361.1556	61.0000	0.29781
511.8100	0.24000	384.2080	62.0000	0.26002
476.2650	0.20000	412.4302	63.0000	0.22207
440.7201	0.16000	448.1699	64.0000	0.18396
405.1751	0.12000	495.7559	66.0000	0.14486
369.6301	0.08000	564.0678	69.0000	0.10458
334.0852	0.04000	677.4754	74.0000	0.06202
298.5402	0.00000	989.0438	90.0000	0.00869

SUBCOOLED

HO	GM	PM	QLE	GBM
298.4355	984.8863	89.5000	0.00902	
277.7292		75.0000		3636.8185
257.1734		55.5000		4879.1381
236.7462		40.0000		5695.8158
216.4284		28.5000		6248.0554
196.2024		19.5000		6661.2808
176.0516		13.0000		6955.5750
155.9610		8.5000		7161.5603
135.9174		5.5000		7303.3229
115.9095		3.5000		7402.7255
95.9285		2.0000		7483.0891
75.9655		1.0000		7543.0429
56.0130		0.5000		7577.3160

597 191

PO = 200

STEAM DOME

HO	QLI	GM	PM	QLE
1198.3323	1.0000	404.9911	115.0000	0.95840
1164.6192	0.96000	412.6401	116.0000	0.92263
1130.9062	0.92000	420.7460	116.0000	0.88628
1097.1932	0.88000	429.3486	116.0000	0.84993
1063.4801	0.84000	438.5008	116.0000	0.81357
1029.7671	0.80000	448.2634	116.0000	0.77722
996.0541	0.76000	458.7188	117.0000	0.74114
962.3411	0.72000	469.9450	117.0000	0.70474
928.6280	0.68000	482.0366	117.0000	0.66833
894.9150	0.64000	495.1184	118.0000	0.63205
861.2020	0.60000	509.3398	118.0000	0.59559
827.4889	0.56000	524.8582	118.0000	0.55914
793.7759	0.52000	541.9175	119.0000	0.52265
760.0629	0.48000	560.7505	119.0000	0.48615
726.3499	0.44000	581.7339	120.0000	0.44951
692.6368	0.40000	605.2927	121.0000	0.41278
658.9238	0.36000	632.0075	122.0000	0.37594
625.2108	0.32000	662.6570	123.0000	0.33901
591.4977	0.28000	698.3628	124.0000	0.30198
557.7847	0.24000	740.7081	126.0000	0.26448
524.0717	0.20000	792.0562	128.0000	0.22680
490.3586	0.16000	856.3963	130.0000	0.18893
456.6456	0.12000	940.5868	134.0000	0.14986
422.9326	0.08000	1058.6405	139.0000	0.10992
389.2196	0.04000	1246.1863	149.0000	0.06672
355.5065	0.00000	1677.9457	174.0000	0.01418

SUBCOOLED

HO	GM	PM	QLE	GBM
355.4012	1689.6094	176.5000	0.01265	
334.1763		156.0000		4744.2828
313.1728		120.0000		6439.8882
292.3600		91.5000		7545.7720
271.7132		68.5000		8355.4823
251.2077		50.0000		8973.8619
230.8241		36.0000		9431.6510
210.5445		25.5000		9775.2076
190.3504		17.5000		10042.2253
170.2264		11.5000		10250.7159
150.1582		7.5000		10398.5106
130.1334		4.5000		10519.4758
110.1415		3.0000		10586.7201
90.1748		1.5000		10664.0382
70.2241		0.5000		10729.3969
50.2806		0.5000		10729.3969

597 192

PO = 400

STEAM DOME

HO	QLI	GM	PM	QLE
1204.5891	1.00000	800.6125	232.0000	0.95057
1173.3723	0.96000	815.3308	232.0000	0.91509
1142.1555	0.92000	830.8904	232.0000	0.87962
1110.9387	0.88000	847.3849	233.0000	0.84439
1079.7219	0.84000	864.9036	233.0000	0.80888
1048.5051	0.80000	883.5644	234.0000	0.77356
1017.2882	0.76000	903.4964	235.0000	0.73818
986.0714	0.72000	924.8504	235.0000	0.70261
954.8546	0.68000	947.8042	236.0000	0.66714
923.6378	0.64000	972.5743	237.0000	0.63161
892.4210	0.60000	999.4087	238.0000	0.59601
861.2042	0.56000	1028.6131	239.0000	0.56035
829.9874	0.52000	1060.5820	240.0000	0.52464
798.7706	0.48000	1095.7591	242.0000	0.48880
767.5538	0.44000	1134.7449	242.0000	0.45303
736.3370	0.40000	1178.2655	244.0000	0.41701
705.1202	0.36000	1227.3554	246.0000	0.38088
673.9034	0.32000	1283.2825	249.0000	0.34445
642.6866	0.28000	1347.8150	251.0000	0.30806
611.4698	0.24000	1423.5836	255.0000	0.27108
580.2529	0.20000	1514.3767	259.0000	0.23387
549.0361	0.16000	1626.0762	263.0000	0.19643
517.8193	0.12000	1769.0988	272.0000	0.15720
486.6025	0.08000	1962.8817	283.0000	0.11683
455.3857	0.04000	2252.8882	298.0000	0.07446
424.1689	0.00000	2810.5223	336.0000	0.02281

SUBCOOLED

HO	GM	PM	QLE	GBM
424.0582	2818.8928	338.5000	0.02176	
401.9112		323.0000		6130.3812
380.1244		259.0000		8362.8217
358.6411		205.5000		9896.1754
337.4160		161.0000		11047.7030
316.4134		124.5000		11940.1259
295.6010		94.5000		12653.0251
274.9535		71.0000		13207.1949
254.4496		52.0000		13659.5830
234.0686		37.5000		14013.8501
213.7919		26.5000		14294.0878
193.6026		18.5000		14510.1471
173.4848		12.5000		14685.1980
153.4242		8.0000		14830.8125
133.4083		5.0000		14941.7567
113.4271		3.0000		15028.7747
93.4720		1.5000		15109.6915
73.5348		1.0000		15143.1222
53.6078		0.5000		15183.1630

597 193

LDS:csc/20K3

PO = 600

STEAM DOME

HO	QLI	GM	PM	QLE
1203.6560	1.00000	1198.6280	349.0000	0.94281
1174.3777	0.96000	1220.1341	349.0000	0.90809
1145.0095	0.92000	1242.8471	350.0000	0.87357
1115.8212	0.88000	1266.8888	351.0000	0.83901
1086.5430	0.84000	1292.3870	352.0000	0.80440
1057.2647	0.80000	1319.5053	353.0000	0.76975
1027.9865	0.76000	1348.4202	354.0000	0.73505
998.7082	0.72000	1379.3380	355.0000	0.70031
969.4300	0.68000	1412.5106	356.0000	0.66552
940.1517	0.64000	1448.2129	357.0000	0.63068
910.8734	0.60000	1486.8056	359.0000	0.59582
881.5952	0.56000	1528.7052	361.0000	0.56086
852.3169	0.52000	1574.4021	363.0000	0.52582
823.0387	0.48000	1624.5324	365.0000	0.49068
793.7604	0.44000	1679.8829	367.0000	0.45545
764.4822	0.40000	1741.4174	370.0000	0.42004
735.2039	0.36000	1810.4236	373.0000	0.38450
705.9256	0.32000	1888.5701	376.0000	0.34882
676.6474	0.28000	1978.2159	381.0000	0.31269
647.3691	0.24000	2082.4625	385.0000	0.27652
618.0909	0.20000	2206.0445	391.0000	0.23977
588.8126	0.16000	2356.2594	400.0000	0.20209
559.5344	0.12000	2544.7552	412.0000	0.16330
530.2561	0.08000	2793.7370	427.0000	0.12323
500.9778	0.04000	3150.2029	450.0000	0.08032
471.6996	0.00000	3759.9063	492.0000	0.03092

SUBCOOLED

HO	GM	PM	QLE	GBM
471.5836	3766.8044	495.0000	0.02989	
448.5145		494.0000		7060.0314
425.9657		404.0000		9690.8485
403.8434		327.0000		11537.6085
382.0750		262.5000		12932.3896
360.6086		208.5000		14033.9479
339.3981		163.5000		14923.8848
318.4064		126.5000		15647.2990
297.6048		96.5000		16236.4663
276.9675		72.5000		16716.6492
256.4726		53.5000		17109.3225
236.1013		38.5000		17434.4019
215.8333		27.5000		17688.3306
195.6529		19.0000		17901.0759
175.5443		12.5000		18082.0593
155.4945		8.5000		18208.5132
135.4894		5.0000		18338.4065
115.5197		3.0000		18429.5818
95.5771		1.5000		18517.1230
75.6545		1.0000		18554.2065
55.7435		0.5000		18599.3794

597 194

PO = 800

STEAM DOME

HO	QLI	GM	PM	QLE
1139.3852	1.00000	1601.8977	467.0000	0.93483
1171.8026	0.96000	1629.9740	468.0000	0.90103
1144.2199	0.92000	1659.5905	469.0000	0.86719
1116.6372	0.88000	1690.8980	470.0000	0.83331
1089.0545	0.84000	1724.0607	471.0000	0.79940
1061.4719	0.80000	1759.2771	473.0000	0.76555
1033.8892	0.76000	1796.7579	474.0000	0.73154
1006.3065	0.72000	1836.7660	475.0000	0.69749
978.7238	0.68000	1879.6159	478.0000	0.66351
951.1412	0.64000	1925.6386	479.0000	0.62935
923.5585	0.60000	1975.2756	481.0000	0.59516
895.9758	0.56000	2029.0095	484.0000	0.56090
868.3931	0.52000	2087.4536	487.0000	0.52652
840.8105	0.48000	2151.3914	489.0000	0.49207
813.2278	0.44000	2221.6874	492.0000	0.45748
785.6451	0.40000	[illegible]99.5358	495.0000	0.42278
758.0624	0.36000	2386.4370	500.0000	0.38777
730.4798	0.32000	2484.3241	506.0000	0.35247
702.8971	0.28000	2595.8665	510.0000	0.31720
675.3144	0.24000	2724.6109	517.0000	0.28134
647.7318	0.20000	2875.8504	527.0000	0.24470
620.1491	0.16000	3057.2753	537.0000	0.20770
592.5664	0.12000	3281.5638	551.0000	0.16952
564.9837	0.18000	3570.6659	571.0000	0.12951
537.4011	0.04000	3969.5847	596.0000	0.08760
509.8184	0.00000	4598.1583	643.0000	0.03926

SUBCOOLED

HO	GM	PM	QLE	GBM
509.6954	4599.8453	646.0000	0.03833	
485.6426		666.0000		7808.9177
462.3010		552.0000		10737.3901
439.5291		453.5000		12817.4548
417.2208		369.5000		14417.1921
395.2975		298.5000		15691.9110
373.6997		238.5000		16734.9841
352.3750		188.5000		17592.6584
331.2859		147.0000		18305.6648
310.4010		113.0000		18898.5032
289.6915		85.5000		19391.3306
269.1344		64.0000		19792.3354
248.7106		47.0000		20126.7449
228.3993		33.5000		20411.4873
208.1841		23.5000		20641.9126
188.0502		16.0000		20834.6799
167.9807		10.5000		20996.6174
147.9632		7.0000		21117.1968
127.9873		4.0000		21243.0747
108.0446		2.5000		21322.3916
88.1255		1.5000		21388.4294
68.2244		0.5000		21478.9524

PO = 1000

STEAM DOME

HO	QLI	GM	PM	QLE
1192.9348	1.00000	2012.2927	586.0000	0.92624
1166.9201	0.96000	2046.7310	587.0000	0.89316
1140.9054	0.92000	2083.0151	589.0000	0.86019
1114.8907	0.88000	2121.3189	591.0000	0.82716
1088.8760	0.84000	2161.8434	592.0000	0.79395
1062.8613	0.80000	2204.7964	593.0000	0.76070
1036.8467	0.76000	2250.4569	596.0000	0.72758
1010.8320	0.72000	2299.1033	599.0000	0.69436
984.8173	0.68000	2351.1008	600.0000	0.66095
958.8026	0.64000	2406.8358	603.0000	0.62757
932.7879	0.60000	2466.8086	605.0000	0.59407
906.7733	0.56000	2531.5530	608.0000	0.56050
880.7586	0.52000	2601.8217	612.0000	0.52682
854.7439	0.48000	2678.4101	616.0000	0.49300
828.7292	0.44000	2762.3641	620.0000	0.45905
802.7145	0.40000	2854.9411	625.0000	0.42490
776.6998	0.36000	2957.8119	630.0000	0.39059
750.6852	0.32000	3073.1270	637.0000	0.35591
724.6705	0.28000	3203.6497	643.0000	0.32111
698.6558	0.24000	3353.2249	653.0000	0.28559
672.6411	0.20000	3527.2164	662.0000	0.24989
646.6264	0.16000	3733.7677	675.0000	0.21324
620.6117	0.12000	3985.0953	691.0000	0.17562
594.5971	0.08000	4302.4026	712.0000	0.13650
568.5824	0.04000	4725.8312	742.0000	0.09480
542.5677	0.00000	5349.1533	789.0000	0.04826

SUBCOOLED

HO	GM	PM	QLE	GBM
542.4394	5354.2654	792.5000	0.04728	
517.2948		839.5000		8416.5233
493.1074		701.5000		11617.6445
469.6575		583.0000		13882.0126
446.7965		480.5000		15650.8838
424.4142		393.0000		17074.6096
402.4286		318.0000		18255.5742
380.7760		255.0000		19233.2727
359.4042		202.5000		20047.8584
338.2763		158.5000		20738.8613
317.3574		122.5000		21317.7761
296.6183		93.5000		21800.7817
276.0373		70.0000		22211.1865
255.5917		51.5000		22554.7144
235.2636		37.5000		22835.1482
215.0368		26.5000		23076.9878
194.8930		18.0000		23287.1355
174.8193		12.0000		23458.3445
154.8007		8.0000		23592.7053
134.8277		5.0000		23714.5371
114.8884		3.0000		23816.3879
94.9765		1.5000		23917.4829
75.0855		1.0000		23961.3743
55.2095		0.5000		24015.7004

597 198

PO = 1200

STEAM DOME

HO	QLI	GM	PM	QLE
1184.8117	1.00000	2431.4695	707.0000	0.91694
1160.2950	0.96000	2472.0484	709.0000	0.88477
1135.7783	0.92000	2514.7522	711.0000	0.85253
1111.2616	0.88000	2559.7791	712.0000	0.82012
1086.7449	0.84000	2607.3369	714.0000	0.78778
1062.2282	0.80000	2657.6[illegible]7	716.0000	0.75538
1037.7115	0.76000	2711.0918	720.0000	0.72307
1013.1948	0.72000	2767.9049	720.0000	0.69040
988.6781	0.68000	2828.5217	724.0000	0.65791
964.1614	0.64000	2893.3443	727.0000	0.62527
939.6447	0.60000	2962.9444	730.0000	0.59254
915.1279	0.56000	3037.9084	734.0000	0.55972
890.6112	0.52000	3119.0055	738.0000	0.52678
866.0945	0.48000	3207.1339	742.0000	0.49371
841.5778	0.44000	3303.3925	749.0000	0.46039
817.0611	0.40000	3409.0895	754.0000	0.42699
792.5444	0.36000	3526.0767	762.0000	0.39320
768.0277	0.32000	3656.4971	767.0000	0.35945
743.5110	0.28000	3803.1829	775.0000	0.32523
718.9943	0.24000	3970.1049	786.0000	0.29042
694.4776	0.20000	4162.6888	797.0000	0.25527
669.9609	0.16000	4388.5272	814.0000	0.21889
645.4442	0.12000	4659.6316	830.0000	0.18218
620.9275	0.08000	4995.1085	853.0000	0.14372
596.4107	0.04000	5429.0553	888.0000	0.10223
571.8940	0.00000	6035.7411	932.0000	0.05778

SUBCOOLED

HO	GM	PM	QLE	GBM
571.7589	6041.4884	932.0000	0.05758	
545.3754		1013.0000		8952.7666
520.2658		852.5000		12370.5387
496.0989		714.0000		14807.3864
472.6645		593.5000		16725.0950
449.8132		490.0000		18279.2239
427.4359		401.5000		19565.4343
405.4542		325.5000		20653.4263
383.8055		261.5000		21568.3259
362.4369		208.0000		22340.9675
341.3099		163.0000		23004.6526
320.3935		126.5000		23560.2781
299.6571		96.5000		24036.8718
279.0771		72.5000		24439.7224
258.6352		53.5000		24781.3384
238.3102		39.0000		25064.7664
218.0871		27.5000		25313.6941
197.9493		19.0000		25522.0771
177.8806		13.0000		25692.0505
157.8702		8.5000		25843.0715
137.9053		5.5000		25965.5591
117.9753		3.0000		26095.0872
98.0754		2.0000		26163.5269
78.1972		1.0000		26250.5598
58.3356		0.5000		26308.9785

REQUEST 8

Calculation of break flow using the HEM model is dependent on the stagnation pressure and stagnation enthalpy that occurs at the break. Describe in detail the method by which stagnation pressures and enthalpies will be determined to predict break flows for containment analysis. Provide and justify all equations and assumptions. This discussion should include the blowdown code used to predict flow rates into the containment.

RESPONSE TO REQUEST 8

Vessel pressures and enthalpies in the region of a broken pipe are determined by a nodalization of vessel internal compartments for which mass, energy, and state analyses are performed in such programs as CIPT, LAMB, and SAFE, for which the equations already have been justified. The computation of blowdown flow rate is done by tabular interpolation of stagnation pressure and enthalpy occurring in that node directly adjacent to the blowdown flow path.

REQUEST 9

Discuss the effect of break size on the critical flow rate and justify extrapolation of small scale test results to reactor conditions.

RESPONSE TO REQUEST 9

The data of Sozzi and Sutherland in NEDO 13418, Figure 10, and Allemann, Ref. 14. of NEDO-21052, show that increased pipe diameters tend to give lower critical mass fluxes. Although reasons for this behavior are not fully understood, it is expected to be largely caused by two-dimensional effects both in the vessel and the pipe, which are amplified in larger scale. The one-dimensional HEM agrees best with small pipe data and tends to overpredict larger pipe data. Therefore, one should predict conservative blowdown rates from large pipes when using the one-dimensional HEM.

REQUEST 10

NEDO-21052 discusses two critical flow models; the homogeneous equilibrium model and a modified slip-flow model. Discuss the manner by which you intend to apply these two models for containment analysis. In addition, since the HEM model is limited to pipe lengths greater than four inches and less than an equivalent fl/d of three, discuss any limitations on the application of the HEM model to the Mark I, Mark II, or Mark III containment designs with regard to break location assumptions.

RESPONSE TO REQUEST 10

The method proposed to employ the HEM and slip models of NEDO-21052 is this:

The maximum discharge mass flow rate should be determined with the HEM based on vessel stagnation properties near the discharging flow passage for pipes of fL/D less than approximately 3.0. There is no further need to determine slip flow properties at discharge since slip properties will not alter the upstream homogeneous choked conditions. For fL/D greater than about 3.0, the slip model described in APED 4827 should be employed for discharge rates. (The value of fL/D = 3.0 is approximately where a pipe friction model based on slip flow would unchoke the entrance homogeneous condition.) Postulated large pipe breaks in a BWR involves flow paths of sufficient length to establish phase equilibrium, and thus lend themselves to the HEM for a determination of the maximum discharge rate.

SUPPLEMENTARY INFORMATION

NRC request for this information was contained in a letter from D. G. Eisenhut (NRC) to L. J. Sobon (GE) dated January 30, 1978

GE response with the following information was provided in a letter from L. J. Sobon (GE) to D. G. Eisenhut (NRC) dated June 30, 1978

NRC QUESTIONS

REPLY TO NRC REQUEST

FOR ADDITIONAL INFORMATION ON NEDO-21052

Reference: NRC Letter Dated January 30, 1978, D. G. Eisenhut to L. J. Sobon

REQUEST 1(a)

Identify the computer code that will be used to calculate the break flow. Provide documentation or available references which give all of the equations and assumptions used in the code. Where appropriate, provide specific page numbers for the reports referenced.

RESPONSE 1(a)

The computer code used to calculate breakflow for containment analysis is the M3CPT03 code which uses the technology described in NEDO-20533. The pressure vessel model used in these calculations is described in Section 2 (page 2-1 to 2-8) and the details of the pipe inventory model are contained in Appendix B (page B-1 to B-14).

The following discussion provides details of the methods and assumptions used to calculate the short term mass and energy release to the Mark I primary containment for the Design Basis Accident (DBA) recirculation line break.

597 201

I. Background and Definition

Following a postulated instantaneous double-ended guillotine break at the safe-end to pipe weld on the suction side of the recirculation system, fluid discharges from both broken ends at a rate which is choked by the break areas. The initial mass flux is determined from the initial reactor pressure, the subcooled liquid enthalpy in the recirculation system and the Moody Homogeneous Equilibrium Model (HEM). After the initial blowdown periods, the two break flows make step changes to flows which are choked by the minimum flow area in each broken section. During the period of time necessary to deplete the initial subcooled liquid within the jet pump downcomer region and within the broken recirculation loop, the break fluid enthalpy is assumed to remain at the initial value. After the initial subcooled inventory is depleted, the break flow becomes saturated and discharges at the critical flow rate specified by the HEM model when evaluated at the reactor vessel pressure. During the entire blowdown period, the mass and energy release is calculated assuming HEM critical flow from two sections of straight, frictionless pipe. The following procedure summarizes the steps for determining the initial blowdown periods for the broken sections and for determining the subcooled liquid inventory depletion time.

II. Methods

A. Initial Mass Flow Rates

The initial critical mass flux is a specified fraction of the final (steady state) critical mass flux at a given enthalpy and pressure. This ratio of initial-to-final critical mass flux, at any given pressure, is a function of the degree of fluid subcooling at that pressure. The calculational procedure for determining the initial critical flow from each section takes the conservative approach of using a steady state critical mass flux multipler of 0.72, the HEM initial-to-final critical mass flux ratio for saturated liquid at 1000 psia. The initial break mass flux is based upon the reactor vessel steam dome pressure and the core inlet fluid enthalpy at 102% of the maximum licensed core thermal power.

1) Pipe Side Initial Mass Flow Rate

$$\dot{M}_{I,1} = F \times G_M \times A_{BR}$$

Where F = steady state flow multiplier (ratio of initial to quasi - steady flow)

= 0.72 for subcooled liquid flow (HEM)

G_M = HEM critical mass flux, lbm/sec-ft^2

A_{BR} = Pipe flow area at break location, ft^2

2) Safe-End Side Initial Mass Flow Rate

$$\dot{M}_{I,2} = F \times G_M \times A_{BR}$$

3) Total Initial Mass Flow Rate

$$\dot{M}_{I,\,Total} = \dot{M}_{I,1} + \dot{M}_{I,2}$$

B. Initial Mass Flux Duration

1) Pipe Side Initial Mass Flux Duration

For jet pump plants (BWR/3&4), the flow rate from the downstream section (pipe side) of the broken recirculation loop is eventually limited by the total jet pump nozzle flow area. Since the total jet pump nozzle flow area is significantly less than the break area, the final choked flow through the jet pump nozzles is much smaller than the initial choked flow through the pipe break. To account for initial/final blowdown effects and the limiting restriction of the jet pump nozzles, it is conservatively assumed that the break flow is limited by the pipe area at the break location until the initial fluid inventory in the broken recirculation loop is totally depleted. At that time the break flow rate drops to the lower value determined by the total jet pump nozzle flow area.

For plants (BWR/2) not utilizing jet pumps, the duration of the initial critical flow is the time it would take for an unobstructed acoustic wave to travel twice the length of the downstream section of broken pipe (a round trip from the break location to the vessel and back). This acoustic reflection takes approximately 50 milliseconds.

After this period of time, the break flow rate increases (step change) to a critical flow rate determined by either the break area or the discharge side safe-end nozzle flow area, whichever is limiting.

Pipe Side Initial Mass Flux Duration

(BWR 3/4)

a) If $A_{L1}/A_{BR} < F$

Then $t_1 = \dfrac{M_1}{F \times G_M \times A_{BR}}$

(BWR 2)

b) If $A_{L1}/A_{BR} \geq F$

Then $t_1 = \dfrac{2L_1}{C}$

where M_1 = Initial fluid mass occupying the discharge side broken section, lbm.

A_{L1} = Limiting flow area on discharge side broken section, ft^2

L_1 = Length of discharge side section, ft.

C = Sonic speed, ft/sec.

2) Safe-End Side Initial Mass Flux duration

The period of initial blowdown from the upstream, or safe-end, section of the broken line is also determined by the simplified acoustic model described previously. The initial blowdown period is assumed to be the length of time it would take for an acoustic wave to reflect off the vessel penetration.

Safe-End Side Initial Mass Flux Duration

If $A_{L2}/A_{BR} \geq F$

then $t_2 = \frac{2L_2}{C}$

During this initial period, the break flow remains subcooled and the mass flux, G_M, is evaluated based on the reactor vessel pressure and the subcooled enthalpy.

C. Subsequent Mass Flow Rates

Following the initial blowdown periods, the break flows are choked by the limiting flow area in each section. In jet pump plants where the Reactor Water Cleanup (RWCU) system has a pipe which is common to both the broken recirculation loop and the intact loop, there exists a second critical flow path in the pipe section downstream of the break location. The RWCU system penetrates the recirculation loops between the safe-end break and the jet pump nozzles. Since the total jet pump nozzle flow area is small compared to the recirculation line area, the postulated break area will accommodate the additional RWCU pipe flow from the pressurized unbroken recirculation loop. For the plants with the above mentioned RWCU piping, the smallest flow area in the connecting RWCU line is added to the total jet pump nozzle area to obtain the total final critical flow area for the discharge section (pipe side) of the broken loop.

1) Pipe Side Final Mass Flow Rate

$$\dot{M}_{F,1} = G_M \times (A_{L1} + A_{RWCU})$$

where A_{RWCU} = Limiting area in the RWCU system pipe common to both recirculation loops, ft^2.

2) Safe-End Side Final Mass Flow Rate

$$\dot{M}_{F,2} = G_M \times A_{L2}$$

3) Total Final Mass Flow Rate

$$\dot{M}_{F,Total} = \dot{M}_{F,1} + \dot{M}_{F,2}$$

D. Subcooled Liquid Depletion Time

To account for the subcooled liquid initially present within the jet pump downcomer region surrounding the core shroud and within the broken recirculation loop, a subcooled inventory depletion time is calculated considering critical mass flow rates based upon initial reactor conditions. During this subcooled depletion period, M3CPT03 assumes that the break fluid remains (MGC) at the initial break enthalpy.

$$t_{sc} = t_1 + \frac{M_{sc} - [\dot{M}_{I,1}\, t_1 + \dot{M}_{I,2}\, t_2 + \dot{M}_{F,2}\, (t_1 - t_2)]}{\dot{M}_{F,1} + \dot{M}_{F,2}}$$

597 206

M_{sc} = Initial mass of liquid in the jet pump downcomer region and in the broken loop.

E. Saturated Blowdown From Reactor Vessel

Following the depletion of the subcooled liquid inventory, the break flow changes to critical saturated flow governed by transient reactor conditions. This saturated blowdown continues until break uncovery, at which time the break discharge becomes two phase flow.

NOTE: The above response indicates that plants without jet pumps (BWR/2) have slightly different mass flow rate characteristics for the design basis recirculation line break than plants with jet pumps (BWR/3,4). However, during the preparation of plant unique containment response analyses for the Mark I Containment Program, the BWR/2 plants were found to include flow restricting devices (venturis) in the discharge side of the recirculation piping. With these restrictors, the general mass flow rate characteristics for a design basis recirculation line break at the safe end to pipe weld are the same for plants with or without jet pumps, i.e., the flow rate drops from the initial value based on the pipe break area to a lower value determined by the jet pump nozzle flow area (BWR/3,4) or by the restrictor flow area (BWR/2).

597 207

REQUEST 1(b)

The discussion in NEDO-21052 indicates that the use of the HEM model is appropriate to calculate choking at the entrance of pipe sections upstream of full area breaks and would not be appropriate for orifice type breaks. Describe the manner by which split breaks, limited off-set breaks, and similar break configurations, which approximate an orifice geometry, will be analyzed.

RESPONSE 1(b)

The drywell pressurization rate and containment response due to an instantaneous double ended guillotine break at the safe end of the recirculation piping is bounding for Mark I plants. Therefore, no analyses are performed for drywell pressurization rate or containment response which involve breaks having areas smaller than a double-ended guillotine break.

REQUEST 1(c)

Describe the noding arrangement that will be used in the vessel and reactor piping. Discuss the manner by which the conditions determined from this noding arrangement will be used to establish the break flow rate. Discuss whether the HEM flows will be calculated by internal programming or by external calculation.

RESPONSE 1(c)

The M3CPT03 vessel model uses a single node which is assumed to be at saturated conditions. The code establishes break flow using a table lookup at the vessel pressure and enthalpy. To handle subcooled conditions, an enthalpy is inserted which overrides the computed vessel enthalpy. The magnitude of this subcooled enthalpy input is determined from plant steady state energy balances. The duration of subcooled liquid blowdown is based on the time it takes the mass of subcooled liquid in the recirculation system piping and the downcomer region around the jet pumps to be discharged at the inital break flowrate. Once the subcooled liquid is depleted the break flow is calculated based on the saturated properties in the vessel.

REQUEST 1(d)

Discuss the manner by which the break flow rate will be determined during pipe decompression for short-term mass and energy releases (0 to 2 seconds). Justify the application of the model during this time period giving due consideration to the subcooled nature of the fluid and the probable location of the choking plane at the break rather than the pipe entrance. These conditions may cause the fluid to be in a nonequilibrium state. This justification should be supported by comparison with staff-approved analytical models or applicable experimental data.

RESPONSE 1(d)

For the time that it takes the initial inventory to clear from the pipe side of the recirculation system break, the flow is taken as a fraction of the HEM flow corresponding to vessel pressure, the subcooled enthalpy of the fluid in the line and the pipe area at the break location. For liquid breaks (applicable to Mark I), this fraction is 0.72.

For the short side of breaks at the vessel safe end, the fraction 0.72 is also used, but only for the time that it takes a sonic wave (with velocity ~5000 f/s) to travel from the break to the vessel and back to the break.

The conservatism of the 0.72 multiplier combined with the HEM flow model has been verified by comparison of M3CPT03 predicted mass and energy release using these assumptions to RELAP calculations using the Henry-Fauske-Moody flow model. These results are described below.

597 210

I. Mass Release Rates and Break Flow Specific Enthalpies Calculated Using RELAP

Utilizing the data listed in Table 1, a RELAP run was made to calculate the break flow rates and the corresponding fluid enthalpies for 50 seconds following the postulated break. The reactor pressure vessel was modeled after a 218 BWR/6 standard vessel and the recirculation line geometry was that of a typical 218 BWR/5. The RPV and recirculation lines were modeled to account for frictional and geometric losses. Figure 1 shows the nodalization scheme used in the RELAP analysis. Figures 2 through 5 show the break mass flow rates and the corresponding break fluid enthalpies. The results shown in Figures 2 and 3 indicate that the jet pumps uncover at approximately 8 seconds and the safe-end side of the break uncovers at approximately 11 seconds. When uncovery occurs, the break flow quality rapidly increases, as shown in Figures 4 and 5. When the breaks uncover, there are significant reductions in mass and energy release rates, due to the high quality two-phase break flow, accompanied by a rapid depressurization of the vessel.

II. Mass Release Rates and Break Flow Specific Enthalpies Calculated Using M3CPT03/HEM

Mass release rates and break fluid enthalpies were calculated out to 50 seconds by the containment code M3CPT03, using the HEM critical flow option. The RPV (218 BWR/6) and the recirculation loop (218 BWR/5) input data used in the analysis were the same data (Table 1) used in the comparative RELAP analysis. The method and assumptions used in the M3CPT03 analysis are described in Response 1(a). The results of the analysis are shown in Figures 6 and 7. Figure 6 shows that the recirculation line initial fluid inventory is depleted approximately 1.2 seconds following break occurrence. The break flow rate from the pipe side of the break is then limited by the total jet pump nozzle flow area. The RWCU line flow area was not included in these comparative analyses. MSIV closure, starting at 0.5 seconds,

597 211

causes a vessel pressurization which produces an increasing break flow rate until the subcooled liquid inventory is depleted at approximately 10 seconds. The break discharge then changes to critical saturated liquid flow governed by transient reactor conditions. The break uncovers at about 20 seconds and the break flow becomes two-phase for the remainder of the transient. After break uncovery, the vessel rapidly depressurizes. Figure 7 shows the changes in break-specific energy corresponding to the changes in break flow described previously.

III. Integrated Mass and Energy Release Rates From RELAP and M3CPT03/HEM Analysis

The mass release rates and the corresponding break fluid specific enthalpies given in Figures 2 through 5 for RELAP and given in Figures 6 and 7 for M3CPT03/HEM were integrated and the results are shown in Figures 8 and 9. The results show that the total energy release calculated by M3CPT03 is approximately 17 percent higher than the total energy release calculated by the RELAP code. The integrated mass release rates are 4.71×10^5 lbm for M3CPT03 and 4.08×10^5 lbm for RELAP. The energies that would be released to the primary containment over 50 seconds are 2.84×10^8 BTUs for M3CPT03 and 2.43×10^8 BTUs for RELAP.

IV. Applicability of BWR/5 Comparison to BWR/2,3 and 4

The BWR/5 recirculation loop model and the BWR/6 vessel model used in the RELAP analysis are essentially the same as would be used in a similar study of the BWR/3 or BWR/4. There are minor hardware differences such as the number of nozzles in each jet pump, the flow control mechanism and the type of recirculation flow rate measuring device. However, these hardware differences would not impact a RELAP comparison to M3CPT03 because they would not affect the location of the limiting critical flow areas. The flow control

597 212

valve was a minimum of 90 percent open during the reported RELAP analysis and the venturi flow nozzle in BWR/3s and 4s would not represent limiting flow areas in a similar study. In other words, the break flow rates from both broken sections would choke at the same locations (jet pump nozzles and suction side safe-end nozzle) in a BWR/3 or 4 RELAP analysis as in the reported analysis.

There are recirculation loop dimensional variations in BWR/3, 4 and 5. The BWR/5 recirculation loop in the reported study was approximately 100 feet in length from the suction side safe-end nozzle to the vessel penetration at the jet pump end of the loop. The corresponding lengths of piping in BWRs/3 and 4 vary from 106 feet to 119 feet. The BWR/5 recirculation line flow area at the break location was 1.755 ft^2. In BWRs/3 and 4, the corresponding areas vary from 2.24 ft^2 to 3.67 ft^2. In the reported analysis, the total jet pump nozzle flow area in each recirculation loop was 0.35 ft^2. In BWR/3 or 4, the same area ranges from 0.48 ft^2 to 0.78 ft^2.

These dimensional variations would have no impact on a comparative study of RELAP and M3CPT03/HEM because the increases in critical flow areas would have the same relative impact on each code. The critical blowdown rate would increase in direct proportion to the increase in choking area and a comparison of RELAP and M3CPT03 should look relatively the same as the reported comparison.

The vessel initial subcoooled liquid enthalpy used in the reported analyses is approximately the same as the typical core inlet enthalpy for a BWR/3 or 4. Once again, any variation in initial vessel liquid enthalpy would have the same relative effect on the blowdown calculations for both codes.

The noted differences between a BWR/5 and BWRs/3 and 4 would not affect a comparison of RELAP to M3CPT03 since the variations would have the effect of increasing or decreasing the mass and energy release in approximately the same proportion for each code. Therefore, on a comparative basis, the reported results should be applicable to BWRs/3 and 4.

Although the BWR/2 plants do not have jet pumps*, the conclusions made above for BWRs/3 and 4 plants are also valid for BWR/2 plants. If a comparative analysis were made between RELAP and M3CPT03/HEM for a BWR/2 plant, one final limiting critical flow area would result in the broken pipe at some location between the break and the pipe connection to the vessel. M3CPT03 considers only two locations, the pipe area at the break location and the safe-end nozzle at the inlet to the vessel. M3CPT03 uses the smaller of these areas as the final limiting choked flow area. The pipe side initial blowdown period is on the order of 50 milliseconds and, therefore, has no significant impact on M3CPT03 results.

If the pipe area at the break location is the limiting area, there is no reduction in break pressure because M3CPT03 assumes the pipe to have no pressure drop between the vessel and the break location. If the inlet safe-end is limiting, the blowdown pressure will be the same as in the previous case, i.e., the vessel pressure.

In RELAP analysis, it is possible that there would be a choking point somewhere between the inlet safe-end and the break location because RELAP models the variations in geometry (pump, etc.) and friction. If this were the case, the calculated blowdown rate would be less than it would be if calculated at the inlet safe-end because of pressure drop considerations and reduced critical flow area. Also, if RELAP break flow choked at the break location, the critical mass flux would be reduced due to pressure drop considerations. Therefore, compared to M3CPT03, the highest break flow rates that RELAP could calculate would result from choking the final flow rate at the same locations as does M3CPT03. Since, in the BWR/5 analysis using M3CPT03, the calculated blowdown rates were higher than those

*See Figures 10 and 11 for piping schematics of BWRs/2,3,4 and 5.

calculated using RELAP when choking the flow at the same locations for both models, it can be concluded that M3CPT03 would also produce higher mass and energy release rates from the pipe side of a BWR/2. From a comparative standpoint, an M3CPT03/HEM analysis should produce even more conservative results in the case of a BWR/2 than it did in the reported BWR/5 analysis.

V. Conclusions

The reported analysis and the applicability of the comparison to BWRs/2,3 and 4 shows that the method utilizing M3CPT03/HEM for calculating the short-term mass and energy release to the Mark I containment for the DBA would be bounding and conservative relative to the reported RELAP analysis of any Mark I plant. The primary cause of this conservatism is the behavior of the pressure vessel. The standard M3CPT03 analysis forces the breakflow to remain all liquid until 80% of the inventory is depleted. This causes the vessel pressure to remain high. In RELAP, two phase mixture starts to flow when flashing starts to occur in the liquid adjacent to the break. This results in a more rapid depressurization rate. The conclusion is that the whole analysis using HEM and M3CPT03 is conservative relative to the RELAP analysis using the Henry-faushe-Moody flow model. The same relative behavior is expected for all BWRs/2,3 and 4.

NOTE: The above response indicates that plants without jet pumps (BWR/2) have slightly different mass flow rate characteristics for the design basis recirculation line break than plants with jet pumps (BWR/3,4). However, during the preparation of plant unique containment response analyses for the Mark I Containment Program, the BWR/2 plants were found to include flow restricting devices (venturis) in the discharge side of the recirculation piping. With these restrictors, the general mass flow rate characteristics for a design basis recirculation line break at the safe end to pipe weld are the same for plants with or without jet pumps, i.e., the flow rate drops from the initial value based on the pipe break area to a lower value determined by the jet pump nozzle flow area (BWR/3,4) or by the restrictor flow area (BWR/2).

TABLE 1

Reactor Pressure Vessel and Recirculation Loop Data and Initial Conditions (RELAP and M3CPT03)

Initial Reactor Power	2894. MWt
Initial Vessel Dome Pressure	1040. psia
Initial Core Inlet Fluid Enthalpy	527.5 BTU/lbm
Initial Feedwater Enthalpy	399. BTU/lbm
Initial Mass of Liquid in RPV	399,180. lbm
Initial Mass of Vapor in RPV	17,180. lbm
Initial Mass of Liquid in Each Recirculation Loop	129,130. lbm
Initial Steamline Flow Rate	3459. lbm/sec
Mass of Passive Heat Slabs	1,895,564. lbm
Total Fuel Bundle Heat Transfer Area	61,151. ft^2
RPV Inside Diameter	18.17 ft.
RPV Height	69.31 ft.
Recirculation Line Flow Area (At Break)	1.755 ft^2
Total Jet Pump Nozzle Flow Area in Each Recirculation Loop	0.348 ft^2
Decay Heat	ANS-5

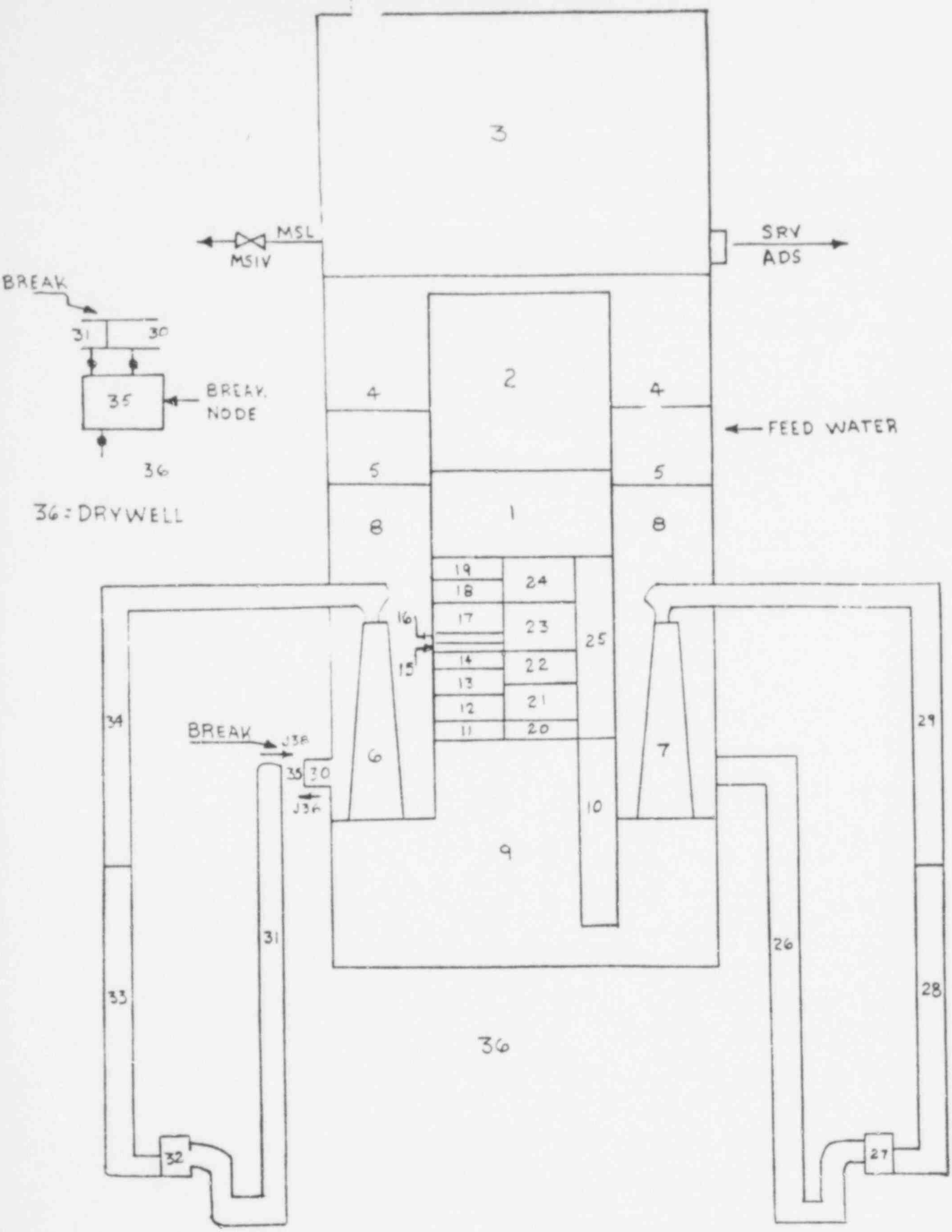

218 BWR/5 RECIRC LINE BREAK

FIG.1 RELAP MODEL

597 217

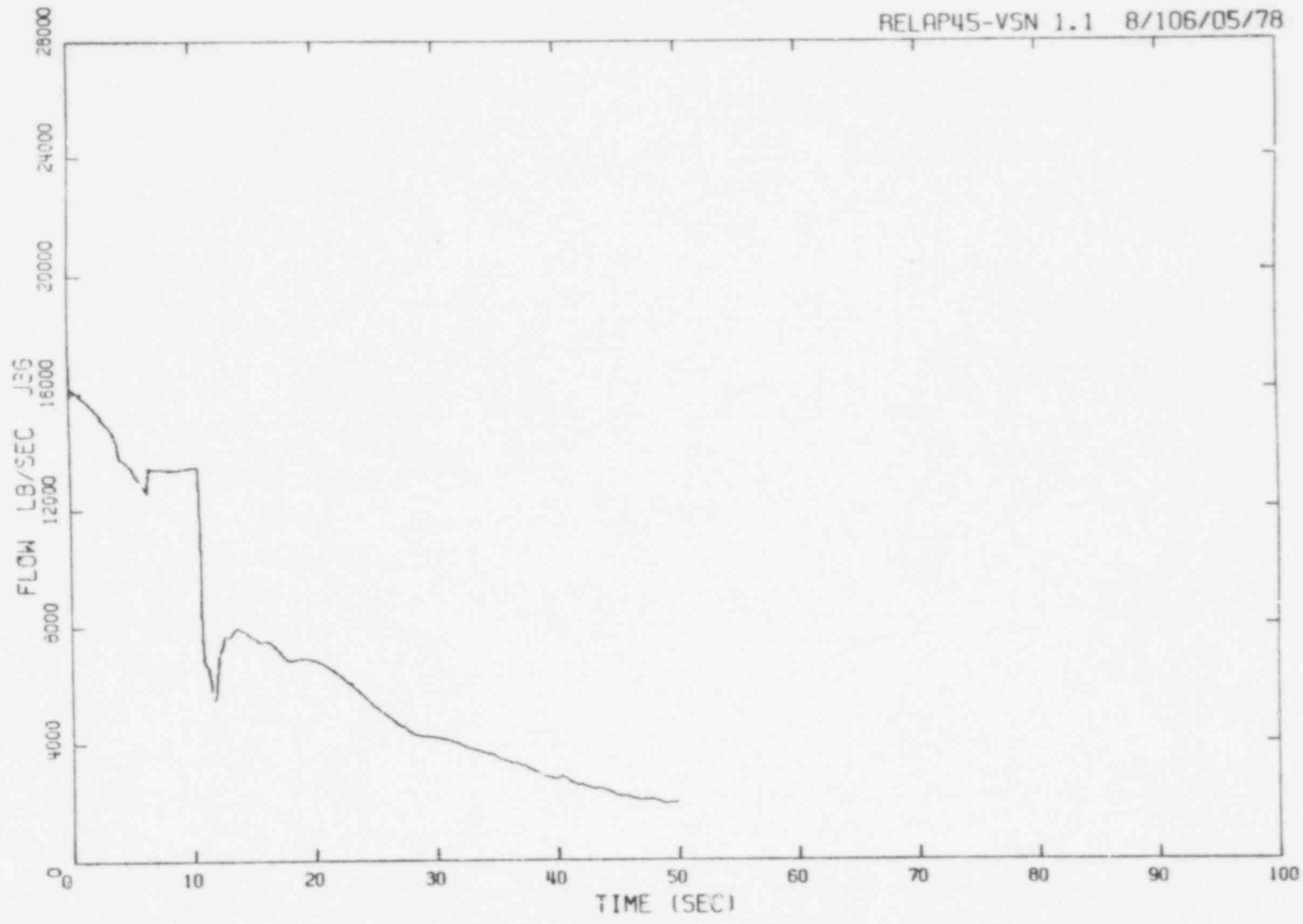

FIG.2 SAFE-END SIDE BREAK FLOW

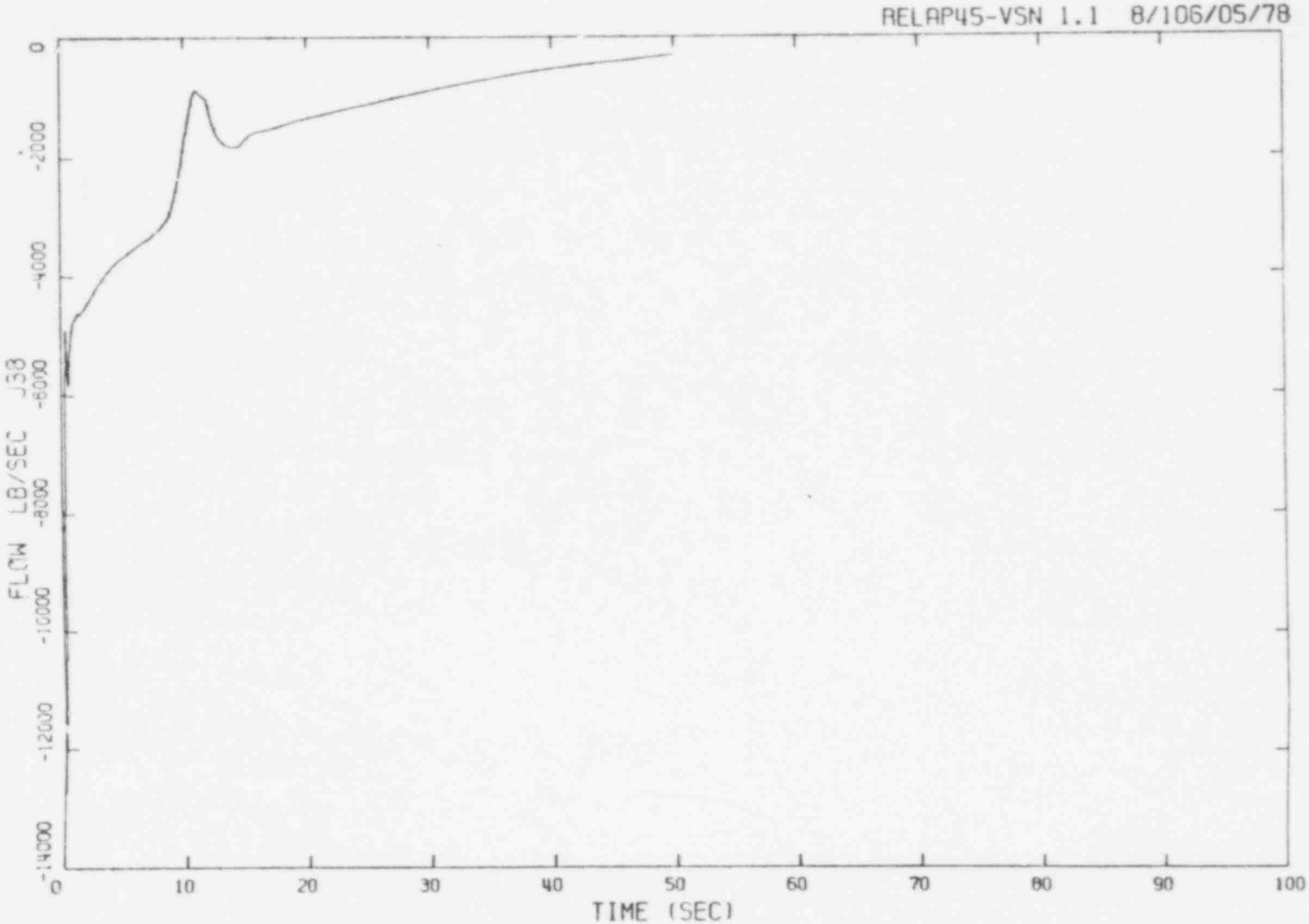

FIG.3 PIPE SIDE BREAK FLOW

597 219

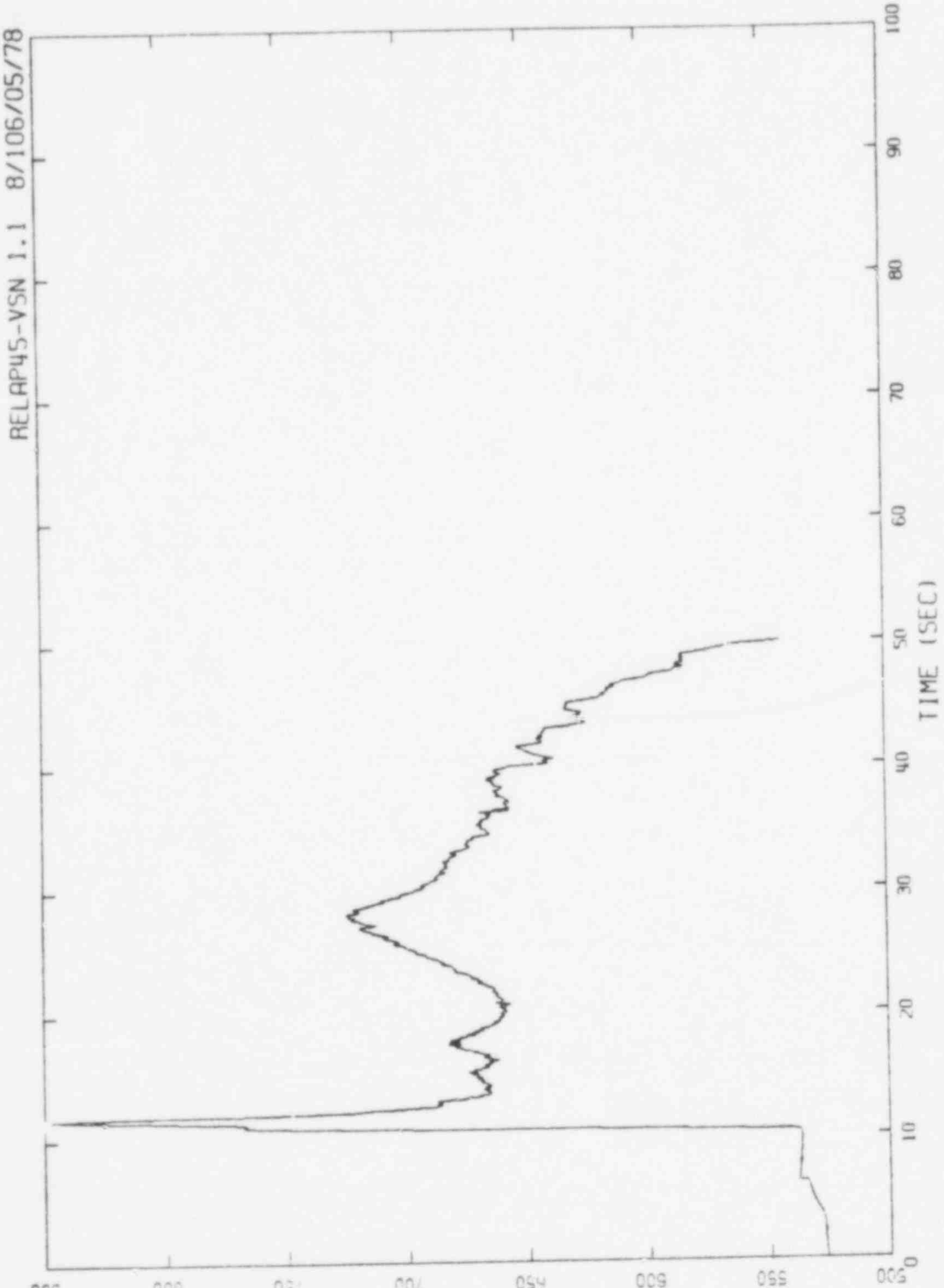

FIG.4 SAFE-END SIDE BREAK ENERGY

597 220

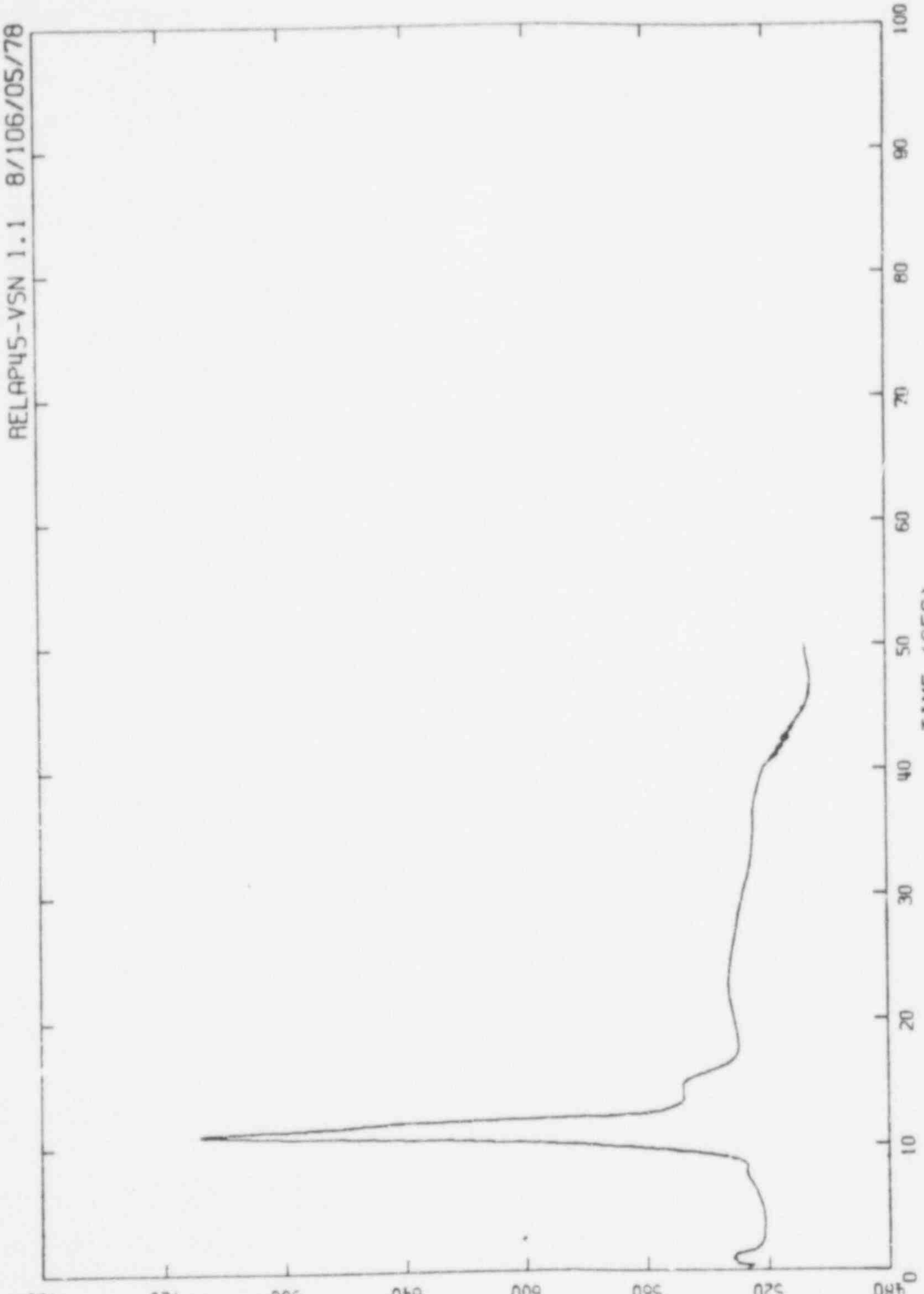

FIG.5 PIPE SIDE BREAK ENERGY

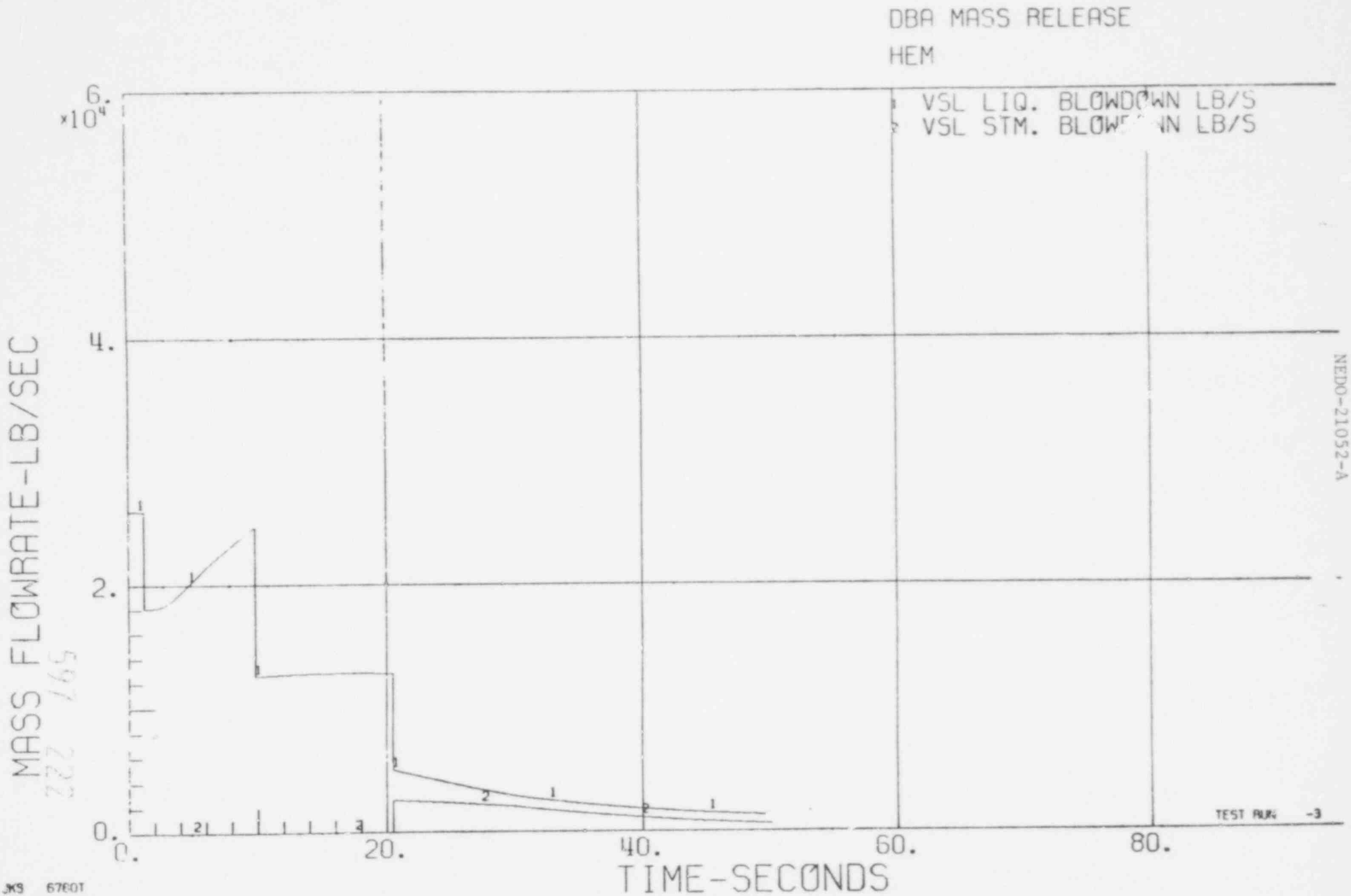

JKS 6760T
06 578 0951.6

FIG.6 TOTAL BREAK FLOW

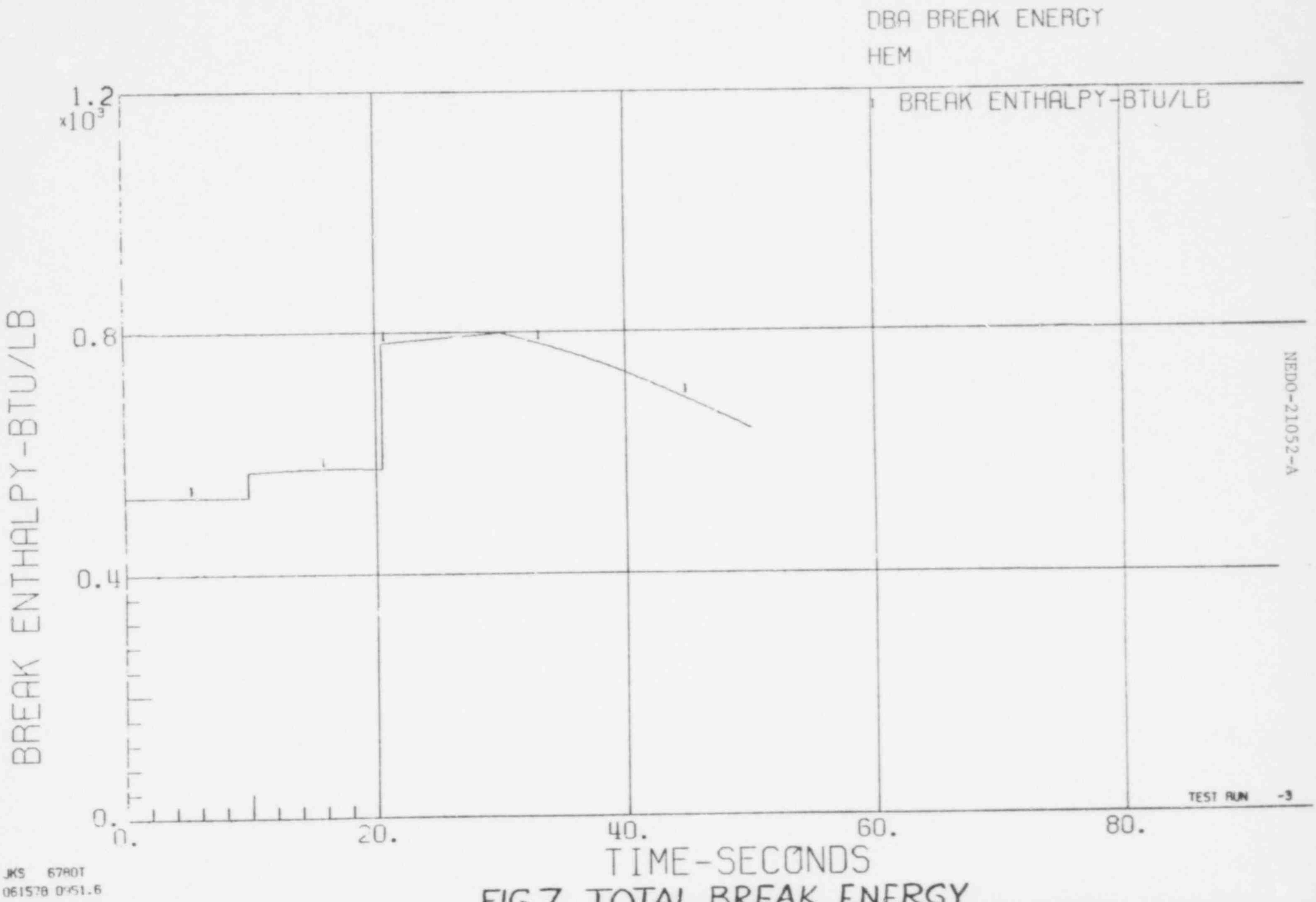

FIG.7 TOTAL BREAK ENERGY

597 223

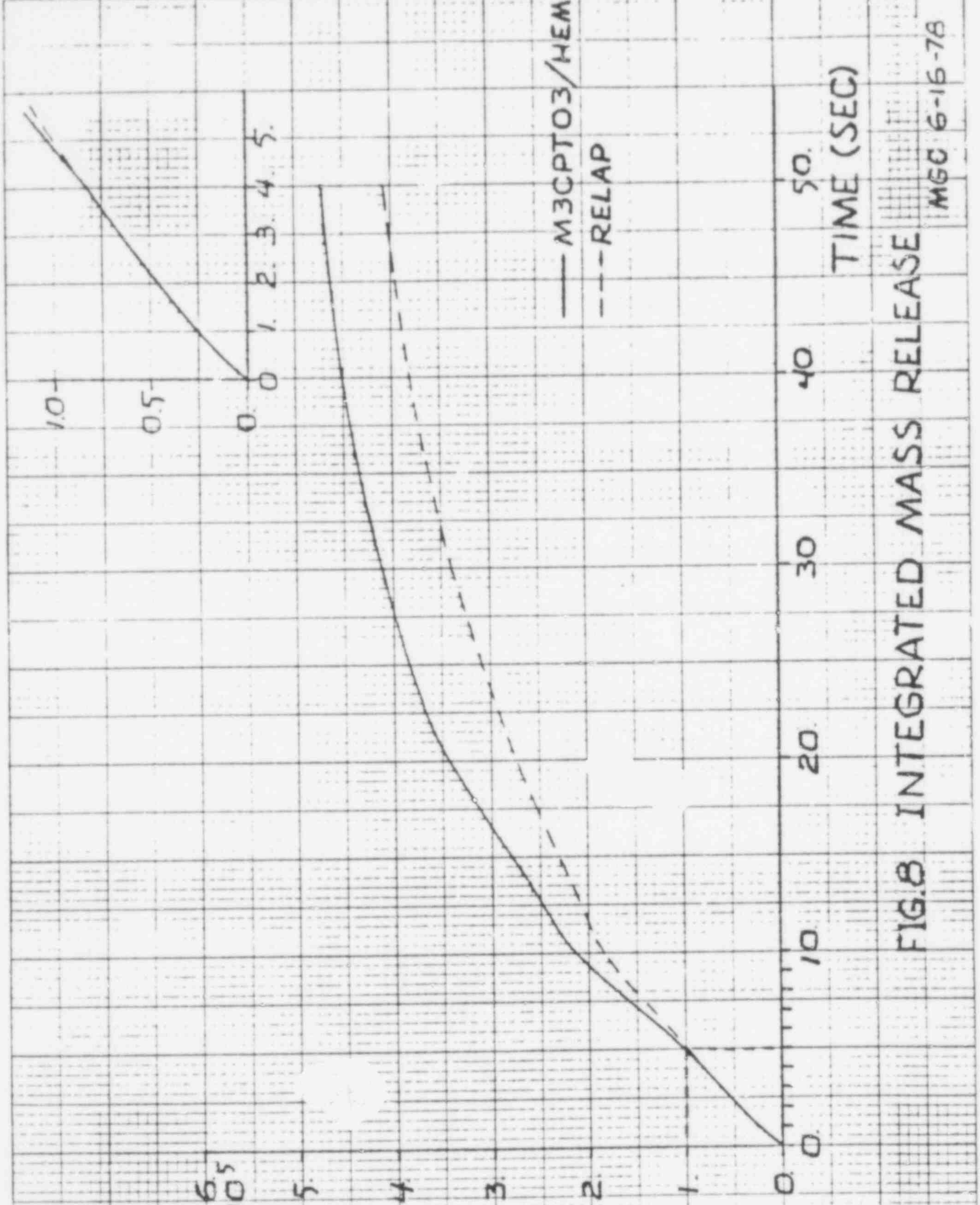

FIG.8 INTEGRATED MASS RELEASE

597 224

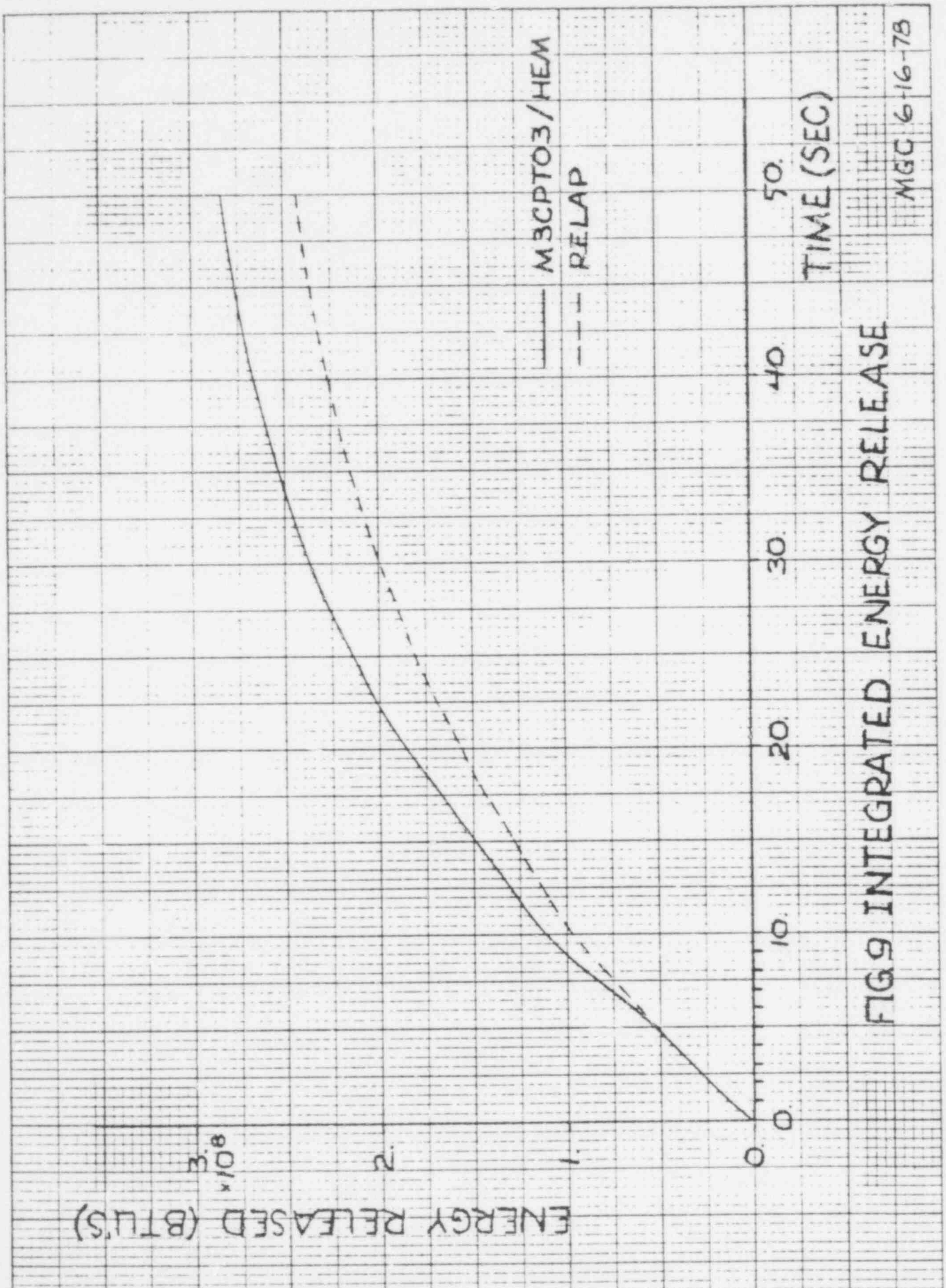

FIG.9 INTEGRATED ENERGY RELEASE

597 225

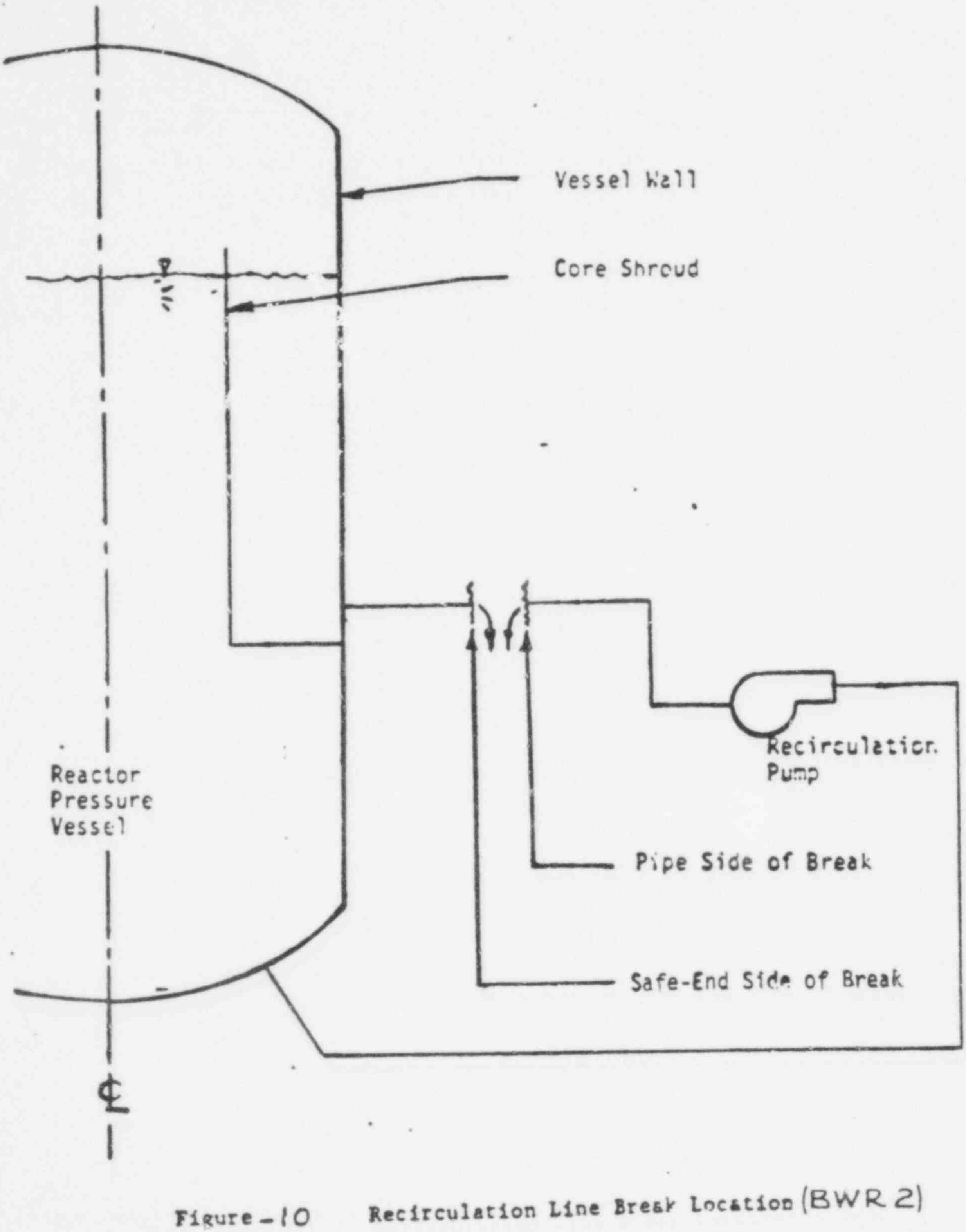

Figure - 10 Recirculation Line Break Location (BWR 2)

597 226

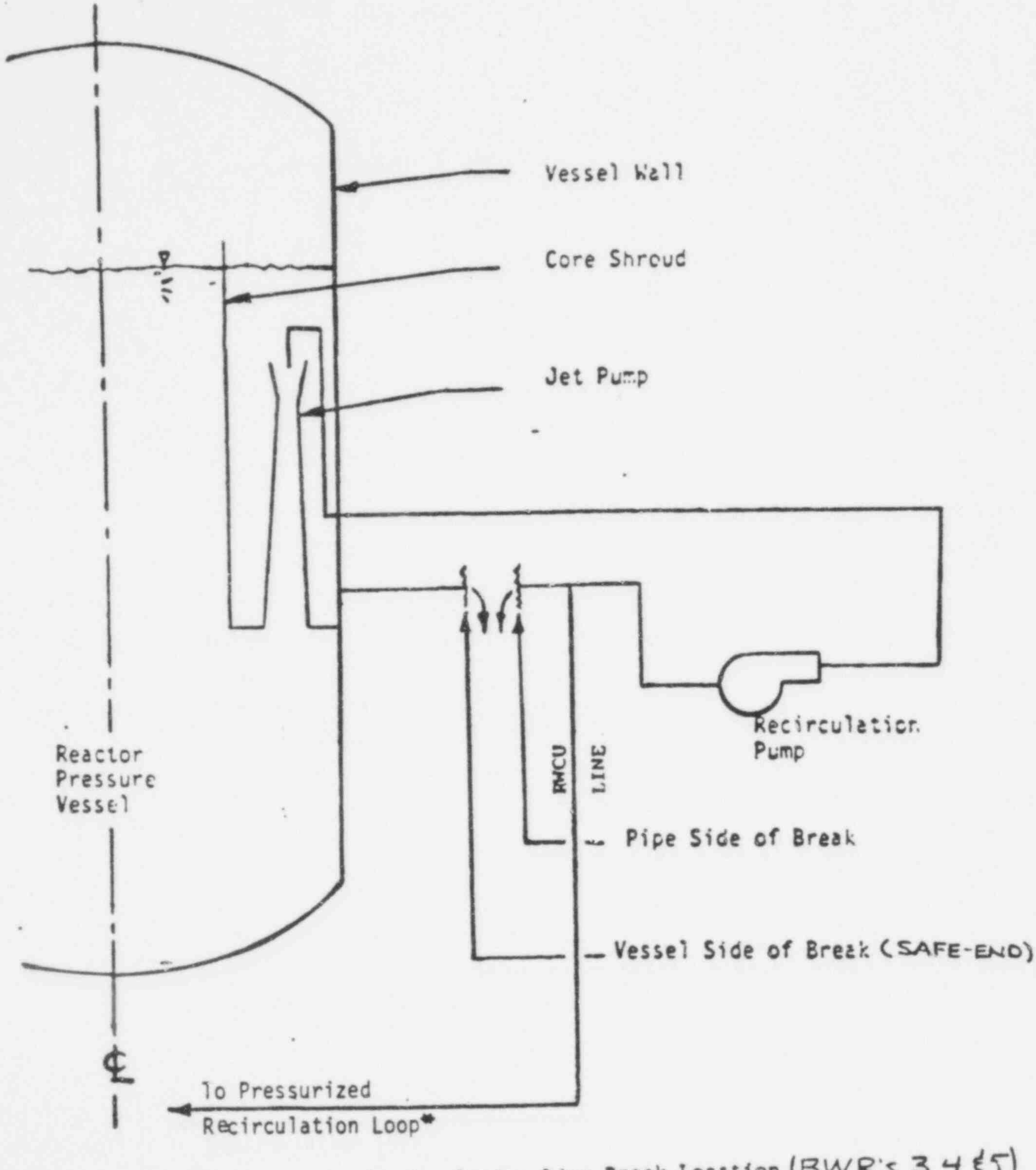

Figure - 11 Recirculation Line Break Location (BWR's 3,4 & 5)

* where applicable

597 227

REQUEST 1(e)

The comparisons of the HEM model with data presented in NEDO-21052 indicate that, for many conditions, the HEM model provides a best estimate rather than a conservative estimate of the break flow rate. Therefore, justify the use of the HEM model as a design tool, for the stagnation pressure and quality range of interest.

RESPONSE 1(e)

There are at least two design philosophies which start at the common basis that some margin of conservatism is essential in nuclear containments.

One philosophy introduces conservatism at all levels of computation or data interpretation so that final design requirements are based on "conservatisms built on conservatisms". Designs based on this philosophy have excessive conservatisms and can be criticized only with regard to economics.

The second philosophy employs the most accurate prediction possible for all interconnected phenomena, finally arriving at an overall "best estimate" for each design parameter. Known degrees of conservatism then are introduced which insures a safe, regulated, design within the framework of competitive economics.

Justification of the HEM as a best estimate design tool becomes one important link in the second philosophy, and represents a desirable step toward improved containment design procedures.

REQUEST 2

Provide a comparison of the break flow as a function of time for a postulated double-ended recirculation line break using both the HEM model and the 1965 Moody frictionless slip flow model in typical BWR/4 plant. The break flow rate should be provided for the first 50 seconds following rupture. Identify the computer code and noding arrangement used in the analysis.

RESPONSE 2

Table 2 presents a comparison of the break flow rates calculated as a function of time using both the slip and HEM models. These calculations were performed for a plant with the typical BWR/5 recirculation system evaluated for Response 1(d). As the discussion in Response 1(d) indicates, the mass and energy release from a break in a BWR/5 is representative of the response for BWRs/2,3 and 4.

The M3CPT03 computer code was used to perform these calculations. The noding arrangement used by this model is described in Response 1(c).

597 229

TABLE 2
HOMOGENEOUS EQUILIBRIUM MODEL BLOWDOWN
FLOW RATES VS MOODY SLIP FLOW RATES
FOR A 218 BWR-5 RECIRCULATION LINE BREAK

HEM			MOODY SLIP FLOW MODEL		
Time (sec)	Blowdown Flow Rates (lb/sec) Liquid	Steam	Time (sec)	Blowdown Flow Rates (lb/sec) Liquid	Steam
0. T 0.00175	21700	0.0	0. T 0.00175	15800	0.0
0.00175 T 1.192	26000	0.0	0.00175 T 1.629	23700	0.0
1.192	18080	0.0	1.629	18900	0.0
5.000	20400	0.0	5.000	20600	0.0
9.808	24600	0.0	9.390	24300	0.0
9.808	12600	0.0	9.390	17800	0.0
20.48	12800	0.0	17.515	17900	0.0
20.49	5020	2610.	17.523	6820	3410.
30.0	2940	2080.	20.0	5780	3210.
40.0	1840	1130.	30.0	2440	2030.
50.0	1280	578.	40.0	1480	855.
			50.0	1880	170.

Bases (HEM):

1) Inventory Flow Multiplier = 0.72

2) Degree of subcooling corresponds to 2894 Mwt.

Bases (Moody):

1) Inventory Flow Multiplier = 0.50

2) Degree of subcooling corresponds to 2894 Mwt.

LJS:att/56
6/30/78

REQUEST 3

It appears that the mass flow rates experimentally determined by Zaloudek ("Steam-Water Critical Flow from High Pressure Systems", HW-80535, January, 1964) and Sozzi and Sutherland ("Critical Flow of Saturated and Subcooled Water at High Pressure", NEDO-13418, July, 1975) are in excess of those calculated by the HEM model when the stagnation conditions approach saturation. Justify the application of the HEM model in this regime.

RESPONSE 3

Comparisons with data of Sozzi and Sutherland shown in NEDO-21052 confirm the best estimate nature of the HEM for both saturated and subcooled stagnation conditions.

The particular Zaloudek data, Figures 2 through 5 of HW-80535 is attached. The solid curve labeled HEM was obtained from Figure 1 in NEDO-21052, employing the values of stagnation enthalpy and upstream (stagnation) pressure given.

It is seen that the HEM gives accurate predictions of all the data presented for both saturated and subcooled stagnation states.

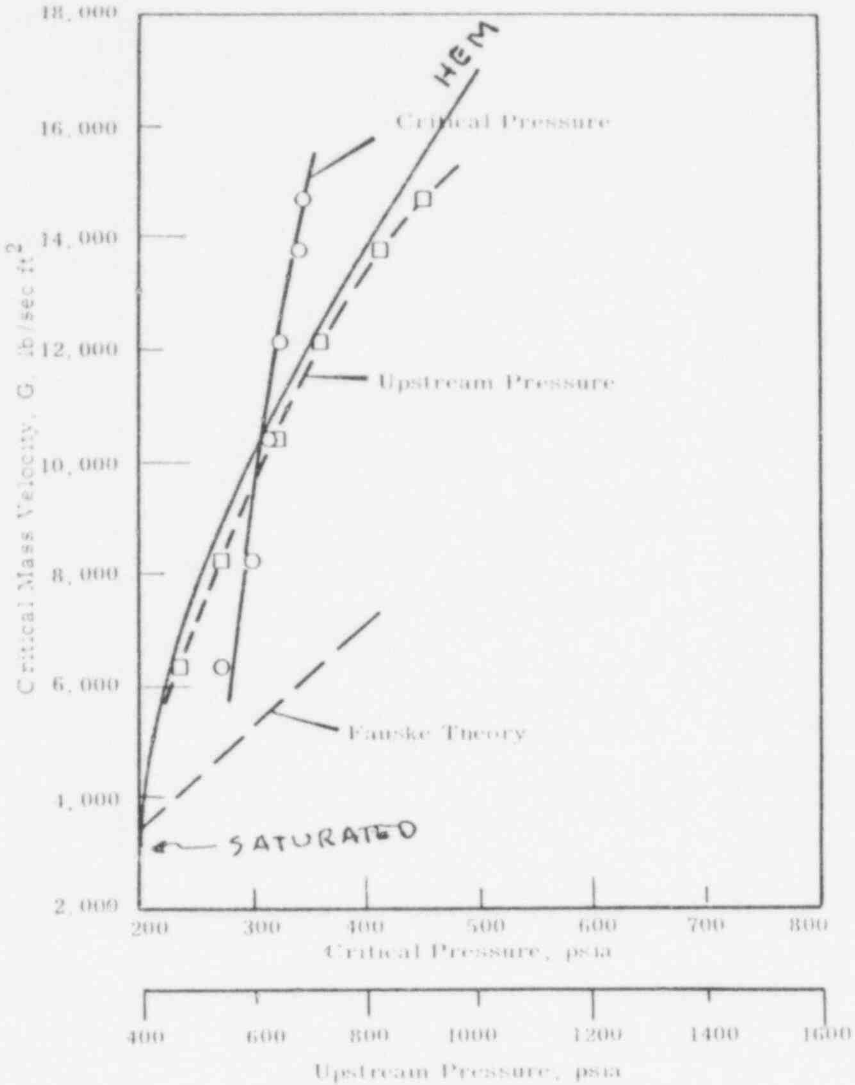

FIGURE 2
Correlation of Data Assuming Choking at Exit of Test Section (E = 421 to 425 Btu/lb)

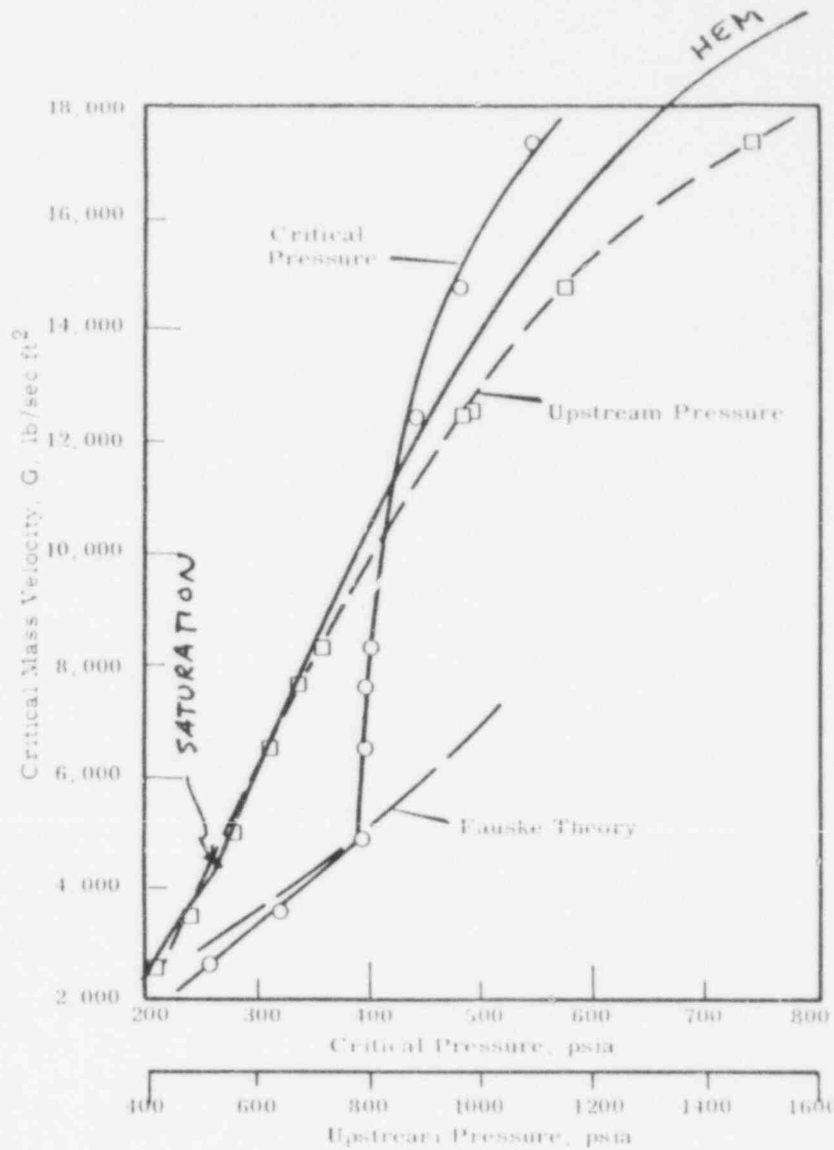

FIGURE 3
Correlation of Data Assuming Choking at Exit of Test Section (E = 463 to 473 Btu/lb)

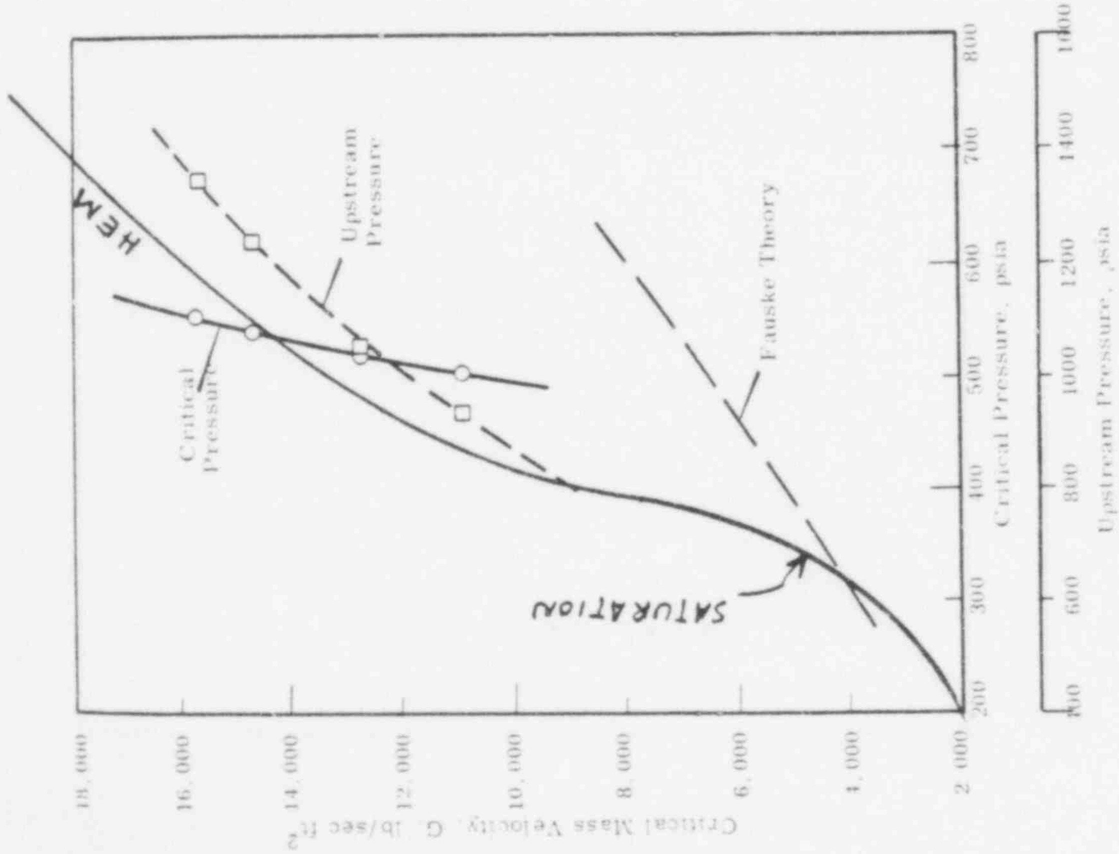

FIGURE 4
Correlation of Data Assuming Choking
at Exit of Test Section
(E = 480 to 490 Btu/lb)

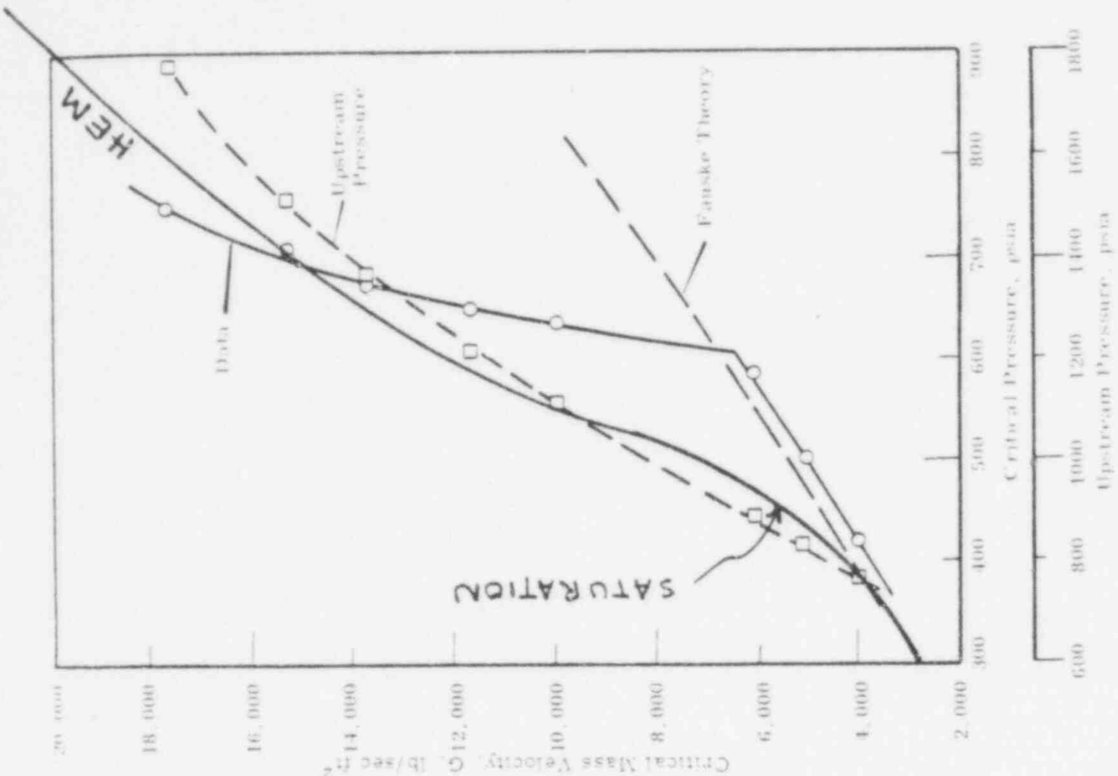

FIGURE 5
Correlation of Data Assuming Choking
at Exit of Test Section
(E = 525 to 533 Btu/lb)

597 233

NRC STAFF TOPICAL REPORT EVALUATION

(Enclosure to December 27, 1978 letter from
D. Eisenhut (NRC) to L. J. Sobon (GE))

597 234

ENCLOSURE

TOPICAL REPORT EVALUATION

REPORT NO.: NEDO - 21052

REPORT TITLE: Maximum Discharge Rate of Liquid-Vapor Mixtures from Vessels

REPORT DATE: September, 1975
ORIGINATING ORGANIZATION: General Electric Company

REVIEWED BY: Analysis Branch, DSS

597 235

SUMMARY OF TOPICAL REPORT

In topical report NEDO-21052 and the additional information provided November 8, 1977, and June 30, 1978, GE has provided a proposed method for predicting break flow for use in containment response analyses. The containment response analysis is used directly in the load combinations for the containment structural assessment and it establishes the boundary conditions for the suppression pool hydrodynamic testing program for plants with Mark 1 containments.

Application of the break flow methods will be limited to double-ended break sizes in the recirculation piping of plants with Mark 1 containments. These are BWR-3's and 4's with jet pumps and BWR-2's without jet pumps. For containments of the Mark 1 design, the first second of blowdown is significant since this is the time period when the vents from the drywell to the suppression pool are clearing. At this time, the maximum structural pool loads are experienced. The first ten seconds of flow are also important since the peak drywell pressure is reached at the end of this period. The pressure response of a typical Mark 1 containment to a postulated recirculation line break is given in Figure 1.

Topical Report NEDO-21052 provides a comparison of the homogeneous equilibrium critical flow model (HEM) with experimental test data. The model was developed using the assumption that the flow process is isentropic and the report provides curves of mass flux as a function of the stagnation enthalpy and pressure. The flow rates are essentially identical to the HEM flow tables contained in the RELAP-4 computer program. For pipes longer than four inches, with low friction, GE concludes that HEM provides a best estimate for prediction of critical flow rates.

A slip flow model is also developed in NEDO-21052 for use with long pipes, but this model will not be used for the prediction of flow rates in the Mark 1 test program. Therefore, this model is not considered in this topical report evaluation.

The additional information provided November 8, 1977 includes tables of HEM flow rates calculated by GE and additional justification for use of the HEM based on experimental test data comparisons.

The information provided June 30, 1978 discusses application of HEM in the M3CPT03 single node blowdown code and provides a comparison of the break flow predicted by M3CPT03 to that predicted by RELAP-4 for a typical BWR with jet pumps. Since the one node M3CPT03 code does not consider local pressure variations when computing the flow from the broken recirculation piping, GE multiples the initial break flow calculated using HEM by a factor of 0.72 for the initial pipe decompression period. The basis for this factor is provided in topical report NEDO-20533 (Ref. 1) and is derived from solution of the mass, energy and momentum conservation equations assuming isentropic flow. The pipe decompression period is about 50 milliseconds for pipes without a restriction between the break and the vessel, and is determined by the time required for a sonic pressure wave to traverse the distance between the break and the vessel and back. The sonic velocity at these conditions is approximately 5000 feet/second.

597 236

For BWR-3's and 4's, the jet pump nozzles provide a large flow restriction at the vessel inlet nozzle. For these plants, the 0.72 factor is utilized for the time required to exhaust the pipe fluid inventory between the break and the jet pump nozzles (about one second). The flow rates during the pipe decompression periods for each side of the break are assumed constant and determined from the HEM tables (flow vs stagnation enthalpy and initial pressure).

Following the initial pipe decompression period, flow rates are determined by HEM, which is programmed into the M3CPT03 code. The code assumes a constant input subcooled enthalpy until the initial subcooled mass of water in the vessel is depleted. After this period, flow rates are determined using the stagnation liquid enthalpy and pressure calculated by M3CPT03. The break flow is assumed to be all liquid until the reactor system inventory is 80% exhausted. Since critical flow rates for liquids are larger than those for two-phase mixtures, these assumptions act to maximize the release to the containment. The switch to two-phase flow is made at about 20 seconds into the transient which is well beyond the times of peak drywell pressure and pressurization rate.

STAFF EVALUATION

General Electric has presented the homogeneous equilibrium model as a best estimate calculation to be used as part of a method for predicting break flows. They propose to introduce conservatism by use of the non-mechanistic one node blowdown model. In our evaluation, we consider both the comparisons of HEM to available experimental test data, and the application of HEM with GE's methodology to assess the overall conservatism.

A. Verification of HEM Flow Rates by Comparison with Experimental Data

The GE justification for use of HEM in predicting break flow is based primarily on the data of Sozzi and Sutherland presented in Ref. 2. These experiments involved the blowdown of a vessel through various nozzles of varying length and diameter. The effect of increased nozzle length was found to decrease the flow rate. A large sensitivity was observed for nozzles less than four inches in length and a smaller sensitivity was observed for nozzles greater than four inches in length. GE attributes the large sensitivity of short pipes to the non-equilibrium condition of the fluid at the point of discharge. For pipe lengths longer than four inches, they conclude that the fluid will have the opportunity to reach equilibrium before leaving the test section so that the flow rates could be predicted by HEM. Pipe lengths longer than four inches would reduce the flow rate only by the reduced stagnation pressure resulting from the increased frictional pressure drop..

Flow rates predicted by HEM were found to agree with the Sozzi and Sutherland data in Ref. 2 for pipes longer than four inches. The HEM model was also compared in NEDO-21052 to data taken by Uchida, Fauske, Henry, Allemann and Zaloudek. These comparisons also showed that general agreement was obtained for pipe lengths longer than four inches. Most of the data were for small diameter pipes of less than one inch ID. The Allemann data, however, included pipes up to 6.8 inches ID and also showed agreement with the HEM predictions.

The effect of nozzle diameter on break flow was evaluated by Sozzi and Sutherland for pipes less than one inch in diameter and 1.75 inches in length. These results indicated that mass flux decreases as diameter increases. Simon (Ref. 4) evaluated the effect of both length and diameter for nozzles of four inches and smaller. The results are presented here as Figure 2. In these studies, a complex relationship was observed on the effect of both nozzle length and diameter on the break flow. The flow rate was observed to either increase or decrease with increased nozzle diameter as a function of the nozzle length.

These studies indicate that small pipe data may not necessarily be applicable for predicting flows from large diameter pipes. The recirculation line area for plants with MARK 1 containments range from 2 to 4 $ft.^2$ while most of the test data is for pipe diameters in the order of a few inches.

Critical flow data for large area pipe sections from 1 to 2 $ft.^2$ are currently being obtained at the Marviken facility (Ref. 5). Preliminary comparisons of the HEM with data from the first two tests have been made by our consultants at the Brookhaven National Laboratory. Comparison curves are attached as Figure 3 and 4. These figures indicate that HEM underpredicts the data by as much as 40%. The results indicate equilibrium conditions may not be reached for large diameter pipes as was observed by Sozzi and Sutherland for small diameter pipes.

In one location the flow length that is available for choking in the BWR-3 and 4 type plants does not appear to be sufficient to produce equilibrium conditions even for pipes of small diameter. The jet pump nozzles provide a reduction in flow area resembling the geometry of an orifice. For orifices, the data of Sozzi and Sutherland indicate flows in excess of HEM. This is because the short transit time through the test section does not permit steam bubbles to form sufficiently for the equilibrium state to be reached. The fluid is consequently discharged at a lower quality and higher density than would be predicted by equilibrium theory, and mass flow rates in excess of HEM are measured. For sharp-edged orifices, flows about 150% larger than HEM were measured for saturated water at 1000 psi.

Orifice flow data obtained by Silver, Bailey, and Schrock were compared by Collins in Ref. 3 to the predictions of HEM. For flow of saturated water, the data was observed to be about 150% larger than HEM values.

Another experimental data comparison was made by Simon in Ref. 4 utilizing data taken by Uchida, Fauske, Friedrich, Burnell, Forster and Esthemer. For flow of saturated water through an orifice at 1000 psi, flows 150% larger than HEM were also observed. Flow rates were found to decrease as the nozzle lengths increased and converge on HEM for lengths of about eight inches.

The available experimental data indicates that HEM may significantly underpredict flow rates through the jet pump nozzles since they resemble an orifice. However, the jet pump nozzles represent only 20% of the total flow area, and would not produce a major portion of the total break flow.

B. Application of HEM of Prediction of Break Flows

Following a double-ended pipe break, the sudden discharge of fluid will produce a decompression wave which travels down the pipe to the vessel. If the pipe is open to the vessel, a compression wave will be produced at the vessel which then travels to the break. During the period of wave travel, the stagnation condition at the break will be reduced from the original state.

Using the isentropic flow assumption discussed in NEDO-20533, Ref. 1, GE calculated the flow rate during the initial wave propagation period to be 72% of the value obtained using HEM at the original stagnation condition. For the assumed condition of isentropic flow, we obtain similar results using the methods presented by our consultant at BNL in Ref. 6.

For open pipes connected to a vessel, the period of reduced flow is of short duration since the wave propagation speed is approximately the speed of sound for liquids (5000 ft/sec). At this velocity, the time required for the pressure wave to traverse a BWR recirculation pipe would be about 50 milliseconds.

For a pipe which has a blockage at the vessel such as the jet pump nozzles, a wave of reduced magnitude would be reflected from the vessel so that the flow rate will decrease from the initial value. This situation would occur for the recirculation piping of BWR-3's and 4's which enter the reactor vessel through the jet pump nozzles.

Instead of decreasing the flow rate during the initial blowdown period as the pressure in the pipe is reduced, GE proposes to assume that the flow remains constant at the initial value of 0.72 times HEM until the initial pipe inventory is exhausted. This requires about 1.2 seconds. Following this time, the flow is based on 1.0 times HEM using the flow area of jet pump nozzles. The 0.72 factor is larger than the value actually predicted using the methodology of NEDO-20533 since it is based on the assumption that the discharged fluid is saturated. If the actual subcooled state of the fluid in the recirculation piping were utilized, a slightl lower value would be obtained.

For the piping section connected to the vessel at the vessel outlet location, GE will use the 0.72 multiplier only for the brief amount of time required for the acoustic wave to traverse through the piping to the vessel and return. Following this period, a flow rate of 1.0 times HEM and the pipe cross sectional area will be used to compute flow for the duration of the blowdown.

As justification for the reduced flow rate during the pipe decompression period, GE has provided a comparison of break flows using the RELAP-4 code for a typical BWR with jet pumps. The RELAP-4 analysis utilized the Henry-Fauske model to predict break flows when the flow was subcooled and the Moody slip flow model was used to predict flow for saturated fluid conditions.

The flow rates calculated by these models are about 60% higher than HEM for saturated and slightly subcooled conditions typical of a BWR. Comparisons of the RELAP-4 flow models to test data from the Marviken experiments were made by the staff in Ref. 7 and by INEL to Semiscale test data in Ref. 8. These comparisons indicate that the models are conservative.

The BWR RELAP-4 model included a multinode description of the reactor vessel piping. The multinode piping description permits RELAP to calculate the acoustic wave propagation following the break. Since the GE model does not take credit for the depressurization of the line between the break and the jet pumps until the line has been evacuated, the model produced 20% higher flows for this period than RELAP. The comparison of the integrated break flow between RELAP-4 and the GE model is attached as Figure 5.

Following the end of the pipe blowdown period, the GE results continued to be more conservative than the RELAP-4 predictions. This results primarily because GE assumes the fluid leaving the vessel is at the liquid stagnation enthalpy. This enthalpy is lower than the two-phase stagnation enthalpy calculated by the RELAP-4 code. The assumption of an all liquid blowdown increases the break flow calculated using HEM so that by the end of 10 seconds, which is about the time of the peak drywell pressure, the GE prediction still exceed RELAP by 15%. The GE results continued to be higher than RELAP for the remainder of the blowdown. The total mass release in the GE model is higher than the RELAP prediction for the total blowdown because of the conservative treatment of feedwater in the GE model. The feedwater is assumed to be within the reactor vessel at an elevated temperature rather than in the system piping.

STAFF CONCLUSIONS

Based on our comparisons of the HEM to experimental data as discussed in the preceeding evaluation, we cannot conclude that HEM is either a conservative or best estimate method for predicting break flow. The Marviden tests provide a break geometry similar to the vessel outlet side of the postulated break. The evaluations of our consultant at BNL indicate that for these tests flow rates are under-predicted by as much as 40% using HEM. For the vessel inlet side of the break that contains the jet pump nozzles, the flow geometry resembles an orifice. The data in References 2, 3 and 4 indicate that for orifice geometry the flow rates could be in excess of HEM by as much as 150%

GE has utilized HEM in a non-mechanistic reactor system model which does not take credit for pressure reduction in the piping during the early portion of blowdown and conservatively assumes all liquid flow during most of the remainder of the blowdown. By comparison of the mass and energy predictions of the GE model to those of a conservative RELAP-4 analysis, we have concluded that the GE model is conservative for prediction of critical flow rates for a postulated double-ended recirculation line break for BWRs with MARK 1 containments.

The GE methodology on the application of HEM to reactor blowdown is presented in the form of answers to the NRC questions. We require that this and the other supporting material in the letters of November 8, 1977 and June 30, 1978 be incorporated into the approved version of topical report NEDO-21052.

597 241

References

1. W. Bilanim, "The Genral Electric Mark III Pressure Suppression Containment System Analytical Model", General Electric Report NEDO-20533, June 1974.

2. G. L. Sozzi and W. A. Sutherland, "Critical Flow of Saturated and Subcooled Water at High Pressure", General Electric Report NEDO-13418, July 1975.

3. R. L. Collins, "Choked Expansion of Subcooled Water and the I.H.E. Flow Model, ASME Journal of Heat Transfer, Vol. 100, May 1978.

4. U. Simon, "Blowdown Flow Rates of Initially Subcooled Water" ANS Topical Meeting on Water Reactor Safety, CONF-730304, March 1973.

5. L. Ericson et al, "The Marviken Full Scale Critical Flow Tests Interim Reports", Results from tests 1, 2, 3, 4, and 5, 1978, Unpublished.

6. P. G. Kroeger, "The Propagation of Phase-Change Fronts in Moving Fluids," BNL-NUREG-50687, August 1977.

7. W. L. Jensen, NRC Memo, "Preliminary Investigation of Marviken Critical Flow Data", May 1978.

8. Douglas G. Hall, "A Study of Critical Flow Prediction for Semiscale MOD-1 Loss-of-Coolant Accident Experiments, TREE-NUREG-1006, December 1976.

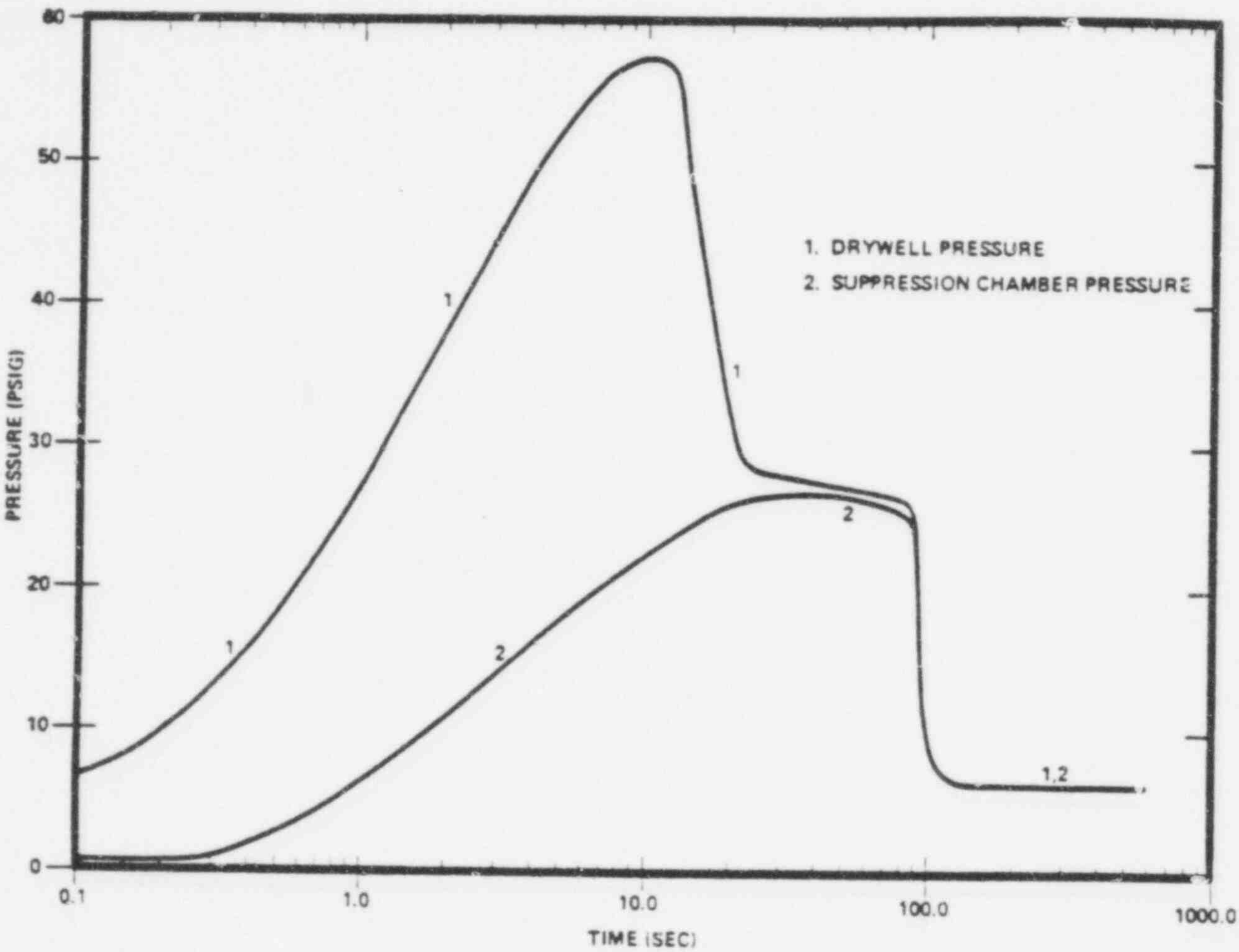

Figure 1 TYPICAL MARK I CONTAINMENT RESPONSE TO A RECIRCULATION LINE BREAK

597 243

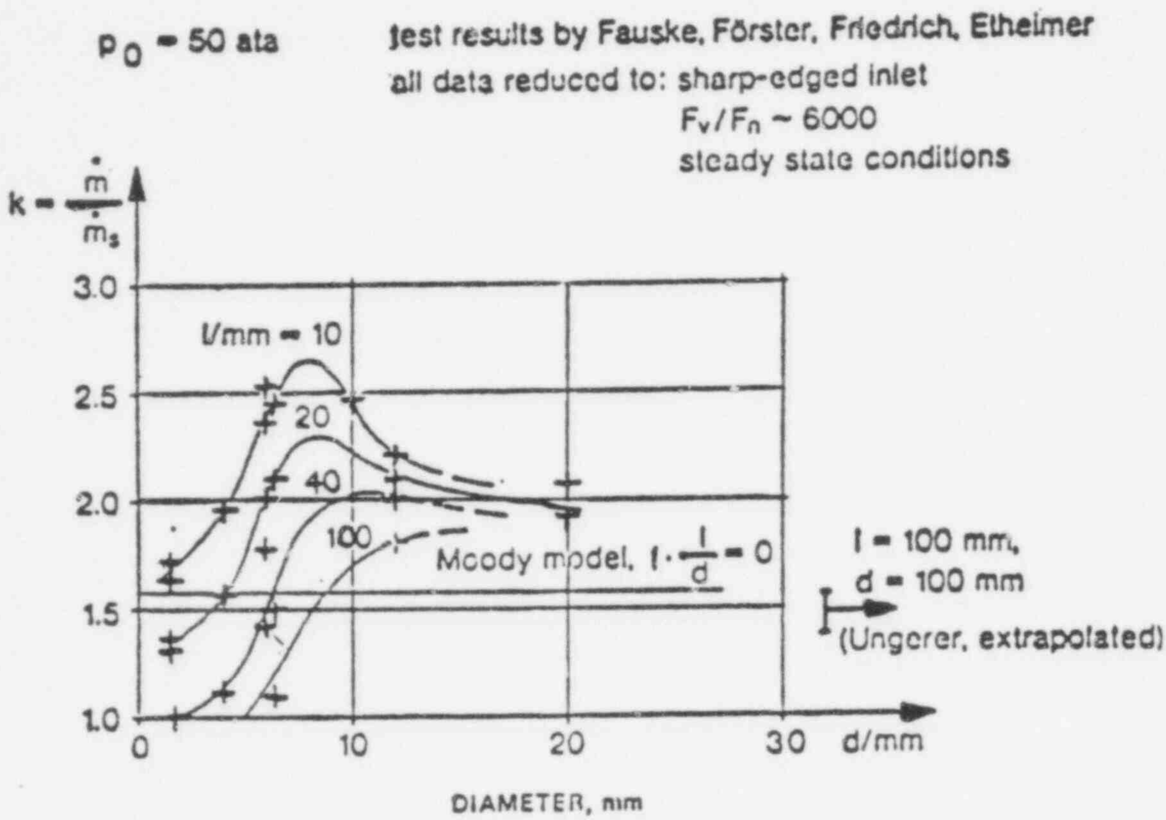

Note: The flow rate k is the measured rate normalized to the HEM value.

Figure 2 FLOW RATE FACTOR RELATED TO NOZZLE GEOMETRY (SHARP-EDGED INLET)

597 244

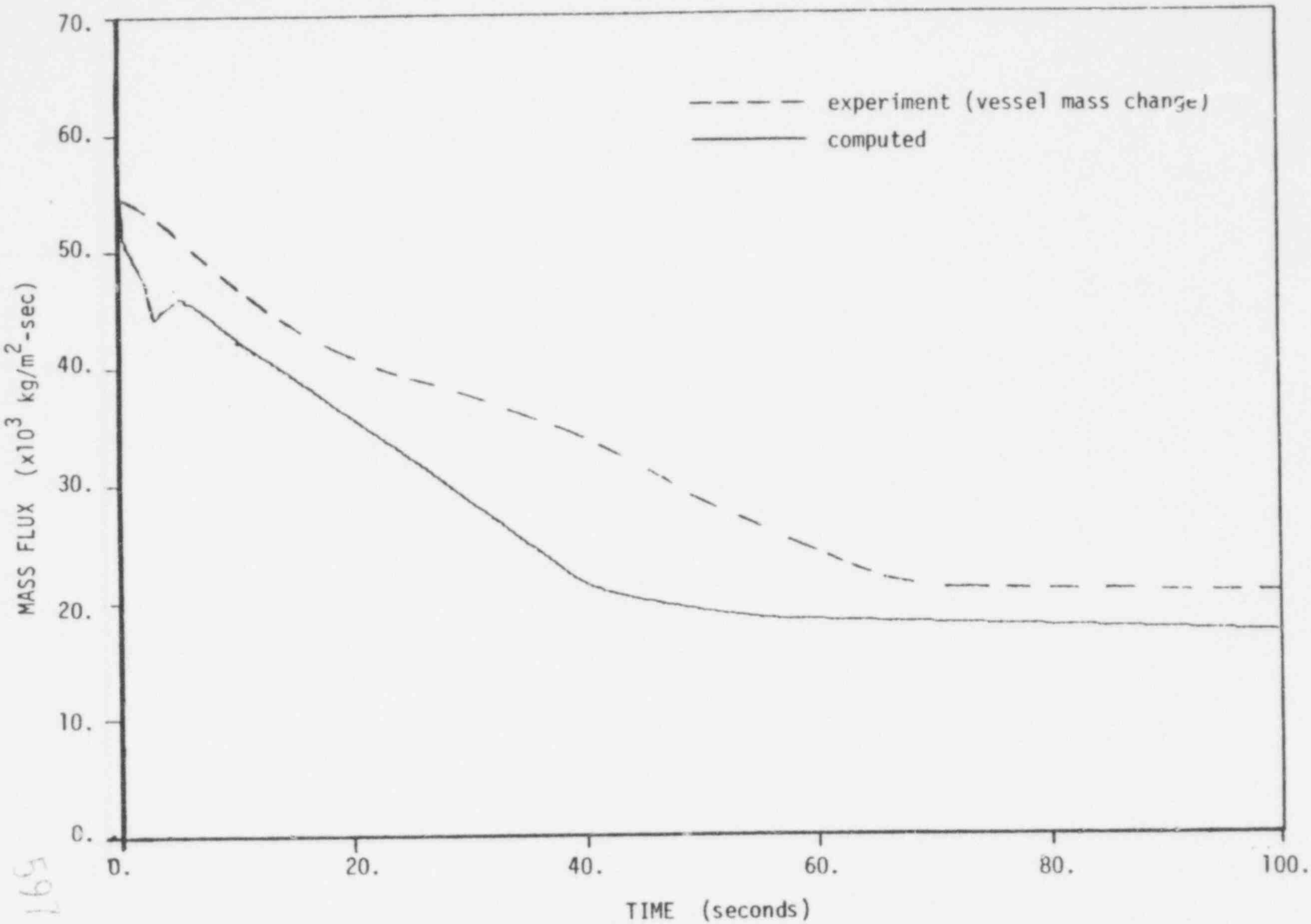

Figure 3 COMPARISON OF COMPUTED AND MEASURED MASS FLUX HISTORIES FOR MARVIKEN TEST NO. 1 (15 C SUBCOOLING), USING A QUASI-STATIONARY ISENTROPIC (IHE) DISCHARGE FLOW MODEL

597 245

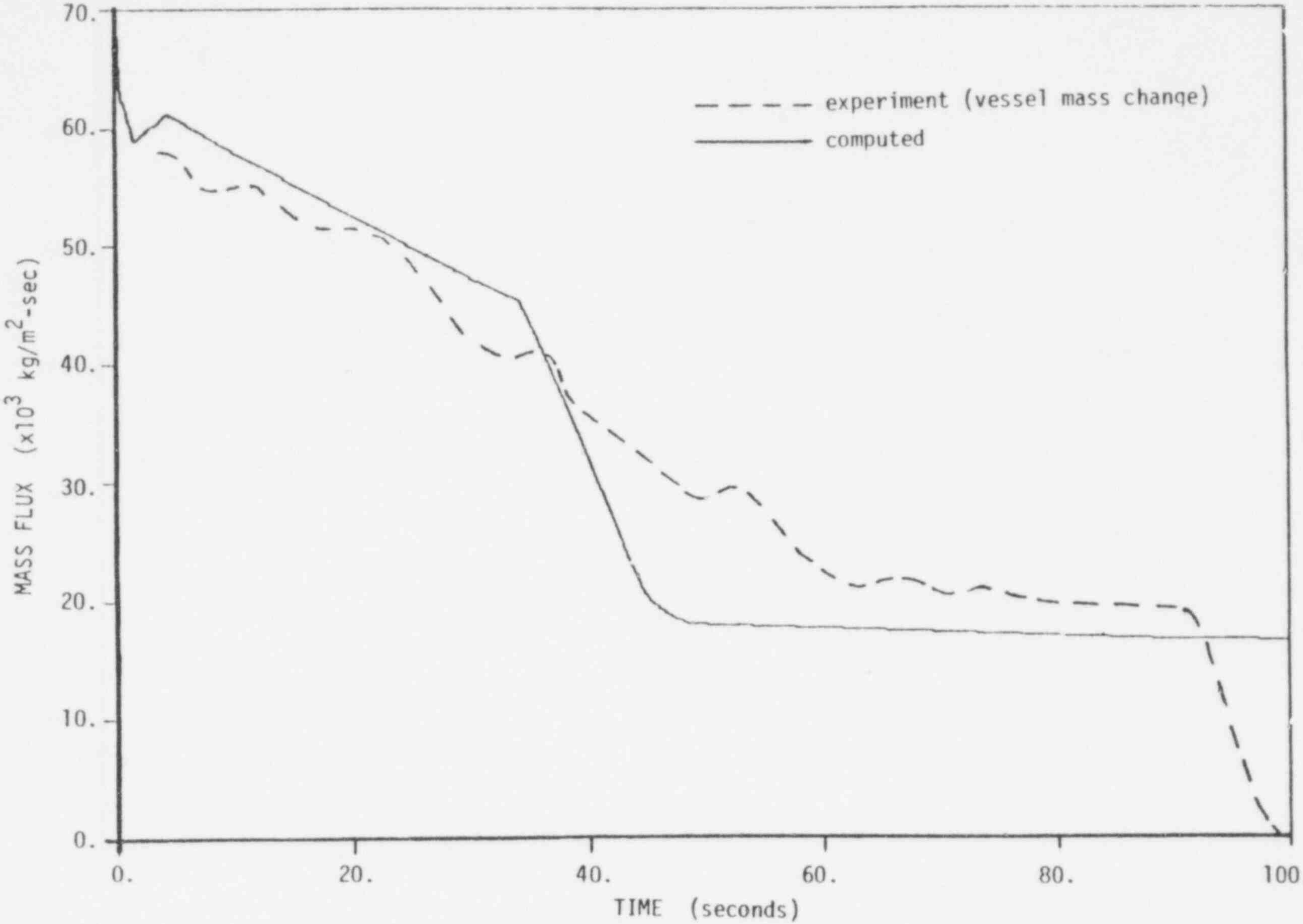

Figure 4 COMPARISON OF COMPUTED AND MEASURED MASS FLUX HISTORIES FOR MARVIKEN TEST NO. 2 (30 C SUBCOOLING), USING A QUASI-STATIONARY ISENTROPIC (IHE) DISCHARGE FLOW MODEL

597 246

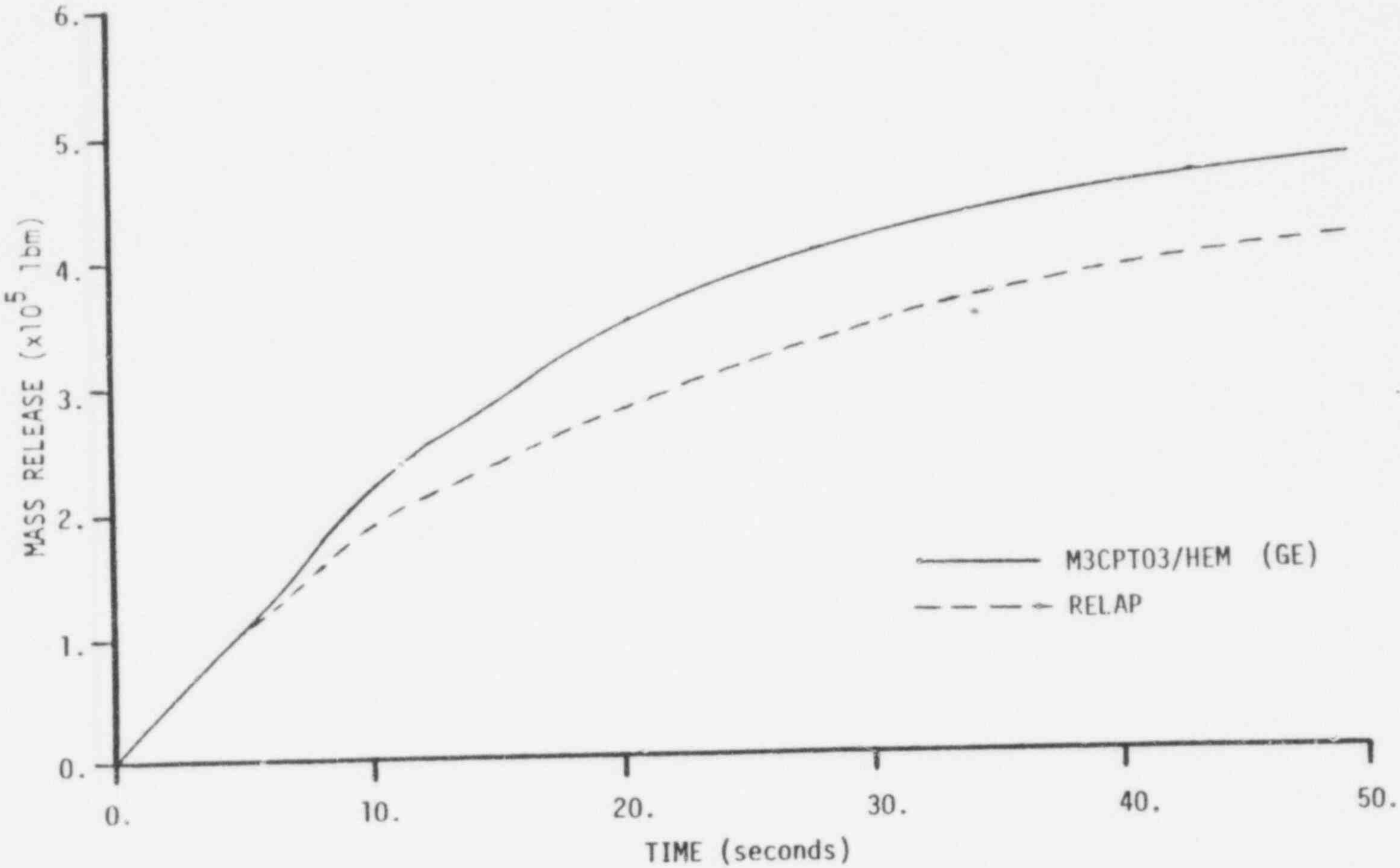

Figure 5 INTEGRATED MASS RELEASE

597 247

NUCLEAR ENERGY DIVISIONS • GENERAL ELECTRIC COMPANY
SAN JOSE, CALIFORNIA 95125

GENERAL ELECTRIC

TECHNICAL INFORMATION EXCHANGE

TITLE PAGE

AUTHOR	SUBJECT	TIE NUMBER
F. J. Moody	730	75NED53
		DATE: May 1979
TITLE: Maximum Discharge Rate of Liquid-Vapor Mixtures from Vessels		GE CLASS: I
		GOVERNMENT CLASS: -
REPRODUCIBLE COPY FILED AT TECHNICAL SUPPORT SERVICES, R&UO, SAN JOSE, CALIFORNIA 95125 (Mail Code 211)		NUMBER OF PAGES: 89

SUMMARY

A discrepancy exists in theoretical predictions of the two-phase equilibrium discharge rate from pipes attached to vessels. Theory which predicts critical flow data in terms of pipe exit pressure and quality severely overpredicts flow rates in terms of vessel fluid properties. This study shows that the discrepancy is explained by the flow pattern. Due to decompression and flashing as fluid accelerates into the pipe entrance, the maximum discharge rate from a vessel is limited by choking of a homogeneous bubbly mixture. The mixture tends toward a slip flow pattern as it travels through the pipe, finally reaching a different choked condition at the pipe exit.

By cutting out this rectangle and folding in half, the above information can be fitted into a standard card file.

597 248

DOCUMENT NUMBER NEDO-21052-A

INFORMATION PREPARED FOR Nuclear Energy Projects Division

SECTION Containment Improvement Programs

BUILDING AND ROOM NUMBER PYD 409 MAIL CODE 905

NED-914 (6/77)

GENERAL ELECTRIC

597 249